Available online at www.sciencedirect.com
ScienceDirect
Computers and Structures 86 (2008) 879–896
Computers & Structures
www.elsevier.com/locate/compstruc

Composite materials non-linear modelling for long fibre-reinforced laminates Continuum basis, computational aspects and validations

Fernando Rastellini *, Sergio Oller, Omar Salomón, Eugenio Oñate

Departamento de Resistencia de Materiales y Estructuras en la Ingeniería, ETSECCPB, Politechnical University of Catalonia, International Center for Numerical Methods in Engineering (CIMNE), Jordi Girona 1-3, Módulo C1 Campus Norte UPC, 08034 Barcelona, Spain

Received 8 March 2007; accepted 30 April 2007
Available online 3 July 2007

Abstract

An innovative computational methodology is proposed for modelling the material non-linear mechanical behaviour of FRP structures. To model a single unidirectional composite lamina, a serial–parallel (SP) continuum approach has been developed assuming that components behave as parallel materials in the fibres alignment direction and as serial materials in orthogonal directions. The model is based on the appropriate management of the constitutive models of the component materials, by making use of suitable 'closure equations' that characterize the composite micro-mechanics [Rastellini F. Modelización numérica de la no-linealidad constitutiva de laminados compuestos. PhD thesis. ETSECCPB, Politechnical University of Catalonia, Barcelona, March, 2006. [in Spanish]]. Classical lamination theory is combined with the SP model to describe multidirectional laminates. The methodology is validated through several numerical analyses, which are contrasted against benchmark tests and experimental data taken from the world-wide failure exercise [Hinton MJ, Soden PD. Predicting failure in composite laminates: The background to the exercise. Comp Sci Technol 1998; 58:1001–10].

Keywords: FRP; Long fibre laminates; Composite failure; Non-linear modelling; FEM

1. Introduction

The use of long fibre composites (LFC) has been extensively developed in the automotive and aeronautical industries during the last 40 years, mainly due to the excellent mechanical properties of this type of materials. During the same period, a great theoretical effort has been made in the analysis of LFC and in the construction of a mathematical basis for the description of their complex micro- and macro-mechanics; consequently, a large amount of literature devising constitutive models for LFC has been produced. Nevertheless, it is remarkable that reliance upon the effectiveness of the failure prediction theories and upon the constitutive models devised in the design of composite structures has not gone hand in hand with the reliance upon the structural properties of this class of materials.

In the last decade, this perspective has begun to change, since the industry demands for improved design methods to reduce the time and cost of bringing new components to the market. Industrial design requires constitutive models that allow realistic structural analysis with degradation of mechanical properties and failure predictions, but at the same time, easy to implement efficiently in an FEM code (finite elements method). An ideal composite model would be the one that could combine already-developed constitutive models (for simple materials) and, at the same time, consider the heterogeneous microstructure. Such a model would make it possible to transfer the large amount of FE

* Corresponding author. Fax: +34 93 401 10 48.
E-mail addresses: frastel@cimne.upc.edu (F. Rastellini), oller@cimne.upc.edu (S. Oller), salomon@cimne.upc.edu (O. Salomón), onate@cimne.upc.edu (E. Oñate).

0045-7949/$ - see front matter
doi:10.1016/j.compstruc.2007.04.009

technology that is currently employed for homogeneous materials. These needs constitute the main motivation of this work, which is to obtain a fast and accurate model to allow reliable numerical simulations of composites. This model would help to predict the ultimate strength of structures and to reduce the expensive experimental testing currently employed in the design practice of components.

The development of a constitutive model for composite laminates is not a simple task since it requires a proper account of the non-linear stress–strain relationships. The lamination sequence obliges us to consider the behaviour of each lamina separately [3], and even the modelling of a single lamina appears to be a complex task since phenomena like fracture, fibre–matrix debonding, micro-buckling and large deformations have to be considered together with their mutual interactions. Puck [4,5] have also remarked that, in the analysis of fibre-reinforced laminates, it is essential to distinguish between fibre failure and matrix failure as well as between fibre degradation and matrix degradation. This observation constitutes a big limitation for those models that consider the composite as an equivalent continuum and accordingly employs exclusively state variables and governing equations which refer to the whole homogenized material. Moreover, as shown by Oller et al. [6,7], the computational cost of a complete double scale approach for a large scale non-linear structural analysis is still not affordable with ordinary computers, even with parallel computations.

The mean-field methods assume that averaged values of the stress and strain states are representative of the behaviour of each phase, and that they are related to the composite stress and strain by mechanical influence functions called concentration tensors. Voigt [8] and Reuss [9] assumed that the strain and stress fields were, respectively, constant in all phases. They proposed simple formulas nowadays-called the rule of mixtures (ROM) and inverse ROM, respectively, to compute the elastic constants of composite.

Classical mixing theory (CMT), whose simpler expression is the ROM, was first studied in 1960 [10] establishing the basis for subsequent developments [11–14]. CMT takes into account the volume fraction of components but not its morphological distribution, since it assumes all component materials experiment the same strain state in all directions (pure parallel behaviour). This feature is a strong limitation for the use of CMT to predict the behaviour of most composites, and consequently modifications to this theory were developed [15,16]. The experience gained in this field with previous research by the authors [17,18] helped to achieve the methodology presented here.

In this paper, within the mean-field approach, a formulation is developed to specifically model the non-linear material behaviour of unidirectional long fibre-reinforced laminas. The aim of the model is to make the composite behaviour dependent on the constitutive laws of component materials according to their volume fractions and to their morphological distribution inside the composite.

The proposed model (for a single lamina) is combined with classical lamination theory to describe laminates consisting of unidirectional continuously reinforced layers.

For validation purposes, the results of several numerical analyses are contrasted with experimental results found in the literature and with the experimental benchmark data [29] provided in the context of the ''world-wide failure exercise''. Recently, the authors employed this model to asses fatigue behaviour of composite fibre-reinforced laminates [20].

2. Numerical model development

The proposed composite model is based on the appropriate management of the constitutive models of component phases within a continuum framework. This model was first sketched by Rastellini and Oller [19] to account for components with additive plasticity and/or damage in elastic stiffness. The generalization presented here allows the compounding of materials with any non-linear constitutive model.

To this end, a preliminary formalization of the multi-material approach denominated 'compounding of material models' is proposed. This may be the basis for future enhancements to take into account different morphological arrangement of the reinforcement by means of proper close equations. Within this framework, two versions of the model are formulated, which basically differ in the closure equations taken into account. Specifically, the former, referred to as the basic serial parallel (BSP) model, inherits closure equations that consider isostrain hypothesis in fibre direction and isostress hypothesis in transversal directions; while the latter, denominated the enriched serial parallel (ESP) model, is devised to improve the transverse and shear stiffness underestimated by the BSP model.

The aim of serial–parallel (SP) models is to help quickly and accurately in the assessment of the non-linear behaviour of composite structures due to material degradation. The consistency of the results is assured by the appropriate election of component material models.

2.1. Basic notations and definitions

It is considered a biphasic fibrous composite material and is postulated the existence, in a statistical sense, of a periodic representative volume element (RVE) with transversely isotropic symmetry. From now on, the two constituent phases will be addressed as 'matrix' and 'fibre', and all the quantities related to them will be denoted by the superscripts m and f.

The reference placement of the composite material body will be denoted by the symbol $\Omega \subset \mathbb{R}^3$. The RVE is classically decomposed as the union of the two non-overlapping subdomains of component materials: $\Omega = {}^m\Omega \cup {}^f\Omega$. We will denote the volumetric fraction by ${}^fk, {}^mk$; evidently ${}^fk + {}^mk = 1$. Average quantities will be used in the subsequent sections. The standard definition of the volumetric

linear average of the strain field for each respective subdomain is

$$\bar{\boldsymbol{\varepsilon}} := \frac{\int_{\Omega} \boldsymbol{\varepsilon}\, \mathrm{d}V}{\int_{\Omega} \mathrm{d}V}, \quad \overline{{}^{f}\boldsymbol{\varepsilon}} := \frac{\int_{f\Omega} \boldsymbol{\varepsilon}\, \mathrm{d}V}{\int_{f\Omega} \mathrm{d}V}, \quad \overline{{}^{m}\boldsymbol{\varepsilon}} := \frac{\int_{m\Omega} \boldsymbol{\varepsilon}\, \mathrm{d}V}{\int_{m\Omega} \mathrm{d}V}. \tag{1}$$

The linear average stresses are defined analogously.

The relationship between average quantities for composite and components is given by the following equations:

$$\bar{\boldsymbol{\varepsilon}} = {}^{f}k^{f}\bar{\boldsymbol{\varepsilon}} + {}^{m}k^{m}\bar{\boldsymbol{\varepsilon}}, \tag{2}$$

$$\bar{\boldsymbol{\sigma}} = {}^{f}k^{f}\bar{\boldsymbol{\sigma}} + {}^{m}k^{m}\bar{\boldsymbol{\sigma}}. \tag{3}$$

Within a strain driven formulation, it is assumed that the current state of the matrix phase in a point $\boldsymbol{x}$ of ${}^{m}\Omega$ is completely defined by the strain in such point ${}^{m}\boldsymbol{\varepsilon}(x)$, and by a finite set of internal variables denoted by the vector ${}^{m}\boldsymbol{\beta} \in {}^{m}\boldsymbol{I}$, where ${}^{m}\boldsymbol{I}$ denotes the set of admissible internal variables. Taking into account that ${}^{m}\boldsymbol{\varepsilon} \in \mathbf{Sym}$, the set of admissible states is

$${}^{m}S = \mathbf{Sym} \times {}^{m}\boldsymbol{I} = \{({}^{m}\boldsymbol{\varepsilon}, {}^{m}\boldsymbol{\beta}) | {}^{m}\boldsymbol{\varepsilon} \in \mathbf{Sym}, {}^{m}\boldsymbol{\beta} \in {}^{m}\boldsymbol{I}\}.$$

The stress ${}^{m}\sigma(\boldsymbol{x})$ is regarded as dependent variable. Constitutive law is stated by the system of differential equations that defines the evolution of the stress and of the internal variables:

$${}^{m}\dot{\sigma} = {}^{m}\boldsymbol{g}({}^{m}\boldsymbol{\varepsilon}, {}^{m}\boldsymbol{\beta}, {}^{m}\dot{\boldsymbol{\varepsilon}}), \tag{4}$$

$${}^{m}\dot{\boldsymbol{\beta}} = {}^{m}\boldsymbol{h}({}^{m}\boldsymbol{\varepsilon}, {}^{m}\boldsymbol{\beta}, {}^{m}\dot{\boldsymbol{\varepsilon}}). \tag{5}$$

In a straightforward way, the previous definitions are extended to the 'fibre' material. The free/elastic energy for unit volume associated with components and composite is denoted respectively by ${}^{m}U$, ${}^{f}U$ and U. The relation between average energies is

$$U = {}^{f}k^{f}U + {}^{m}k^{m}U.$$

2.2. Serial/parallel decomposition

An orthogonal reference frame is used to set the material local basis. Its first axis e_1 is parallel to the axis of cylindrical symmetry (fibre direction). The stress and strain tensor fields considered above are decomposed in what, from now onwards, will be called their respective 'Serial' and 'Parallel' components. Denoting with $\mathbf{N}_{11}$ the projector tensor corresponding to e_1:

$$\mathbf{N}_{11} = e_1 \otimes e_1.$$

It is introduced the fourth order tensor $\mathbb{P}_{\mathrm{P}}$ that recovers the 'parallel component' of stress and strain:

$$\mathbb{P}_{\mathrm{P}} = \mathbf{N}_{11} \otimes \mathbf{N}_{11} \tag{6}$$

and the tensor $\mathbb{P}_{\mathrm{S}}$ that recovers the complementary 'serial component':

$$\mathbb{P}_{\mathrm{S}} = \mathbb{I} - \mathbb{P}_{\mathrm{P}}. \tag{7}$$

Consequently, it may be defined the following 'decomposed' strain and stress fields for the composite:

$$\boldsymbol{\varepsilon}_{\mathrm{P}} = \mathbb{P}_{\mathrm{P}} : \boldsymbol{\varepsilon}, \quad \boldsymbol{\varepsilon}_{\mathrm{S}} = \mathbb{P}_{\mathrm{S}} : \boldsymbol{\varepsilon}, \tag{8}$$

$$\boldsymbol{\sigma}_{\mathrm{P}} = \mathbb{P}_{\mathrm{P}} : \boldsymbol{\sigma}, \quad \boldsymbol{\sigma}_{\mathrm{S}} = \mathbb{P}_{\mathrm{S}} : \boldsymbol{\sigma}. \tag{9}$$

Since parallel and serial components are complementary, one has:

$$\boldsymbol{\varepsilon} = \boldsymbol{\varepsilon}_{\mathrm{P}} + \boldsymbol{\varepsilon}_{\mathrm{S}}, \tag{10}$$

$$\boldsymbol{\sigma} = \boldsymbol{\sigma}_{\mathrm{P}} + \boldsymbol{\sigma}_{\mathrm{S}}. \tag{11}$$

All the previous decompositions and relations are extended to matrix and fibre materials in analogous way.

2.3. Compounding of constitutive models

In this section, it is defined a class (type) of constitutive models for a biphasic composite using the constitutive laws of its compounding materials.

It is first assumed that the set of admissible internal variables of the composite I is formed by the Cartesian product of the sets of state variables of its components ${}^{f}S$, ${}^{m}S$:

$$I = {}^{f}S \times {}^{m}S = \left\{({}^{f}\boldsymbol{\varepsilon}, {}^{m}\boldsymbol{\varepsilon}, {}^{f}\boldsymbol{\beta}, {}^{m}\boldsymbol{\beta}) | ({}^{f}\boldsymbol{\varepsilon}, {}^{f}\boldsymbol{\beta}) \in {}^{f}S, ({}^{m}\boldsymbol{\varepsilon}, {}^{m}\boldsymbol{\beta}) \in {}^{m}S\right\}.$$

The composite internal variables of the new model $({}^{f}\bar{\boldsymbol{\varepsilon}}, {}^{m}\bar{\boldsymbol{\varepsilon}}, {}^{f}\boldsymbol{\beta}, {}^{m}\boldsymbol{\beta}) \in I$, plus the average strain of the composite $\bar{\boldsymbol{\varepsilon}}$, constitute the complete set of state variables of the new constitutive model.

The second assumption is that the constitutive laws of each phase still apply to their corresponding volume-averaged state variables. The model thus defined is governed by Eqs. (2)–(5) plus its 'fibre' counterparts; all written for averaged variables.

It may be seen that the former two assumptions are not sufficient for the definition of a material model. This has a physical base: the definition of a material model for the composite needs the introduction of additional equations that specify somehow the interaction between the component phases. This additional set of equations will be referred to as 'closure equations' and may be expressed in a general form as follows:

$$f_i\left({}^{f}\boldsymbol{\varepsilon}, {}^{m}\bar{\boldsymbol{\varepsilon}}, {}^{f}\boldsymbol{\beta}, {}^{m}\boldsymbol{\beta}, {}^{f}\boldsymbol{\sigma}, {}^{m}\boldsymbol{\sigma}\right) = 0, \quad i = 1, \ldots, 6. \tag{12}$$

Evidently, the resulting material model will depend crucially on the adopted specific closure equation that characterizes the mechanical interaction at the microscale.

This approach essentially converts the problem at the microscale into an algebraic problem. The family of models above defined will be referred to as the *compounding* of constitutive models.

2.4. Closure equations for basic serial–parallel model

The distinctive feature of long fibre composites is the well known strongly anisotropic mechanical behaviour. An appropriate closure equation devised for the specific

problem of unidirectional LFC should possess the following properties: (1) it should retain the essential axial constraint of the phases and maintain the transverse isotropy whenever component materials exhibit this property; (2) it should provide a correct tangent stiffness, which should be equal to the initial elastic one when no-inelastic phenomena have occurred; (3) it should retain a character of simplicity since the convenience of an approximate model, like the one proposed, relies on the possibility of avoiding the complex calculations required by a complete double-scaled analysis; a too complex model would make void the motivation for a simplified analysis.

Furthermore, with the aim of defining a constitutive model whose global algorithm is independent of the specific models of component phases, it will be assumed that the closure Eq. (12) does not depend on the internal variables ${}^f\beta$ and ${}^m\beta$. This requisite implies that the closure equation has to account only for the morphological properties of the unit cell and will have the form:

$$f_i\left({}^f\bar{\boldsymbol{\varepsilon}}, {}^m\bar{\boldsymbol{\varepsilon}}, {}^f\boldsymbol{\sigma}, {}^m\boldsymbol{\sigma}\right) = 0, \quad i = 1, \ldots, 6. \tag{13}$$

The BSP is based on the following closure equation:

$${}^m\bar{\boldsymbol{\varepsilon}}_{\mathrm{P}} = {}^f\bar{\boldsymbol{\varepsilon}}_{\mathrm{P}}, \tag{14}$$

$${}^m\bar{\boldsymbol{\sigma}}_{\mathrm{S}} = {}^f\bar{\boldsymbol{\sigma}}_{\mathrm{S}}. \tag{15}$$

Isostrain in parallel direction and isostress in serial directions are the usual and simpler assumptions when obtaining the properties of composite material; for example, these assumptions were utilized by Dvorak and Bahei-El-Din [21] to define an anisotropic plasticity model, and by Rastellini et al. [17–20] to model the composite behaviour.

Relations (14) and (15) will be henceforth referred to as *basic serial parallel (BSP)* closure equations. It is well known that pure serial behaviour and inverse ROM provide weak estimation of transversal stiffness. The isostress assumption provides transversal stiffness estimates below the lower bound determined by Hill [22] for cylindrical RVE, and is not sufficient for the definition of a realistic model of LFC. To overcome this drawback, the composite model is later improved in Section 2.7 with the enriched SP model.

2.5. Algorithm for the solution of BSP model

The following algorithm is developed for both (basic and enhanced) versions of the model. The only difference is the variables it uses. In the case of BSP, the algorithm make uses of linear average ones ($\boldsymbol{\varepsilon} := \bar{\boldsymbol{\varepsilon}}$, $\boldsymbol{\sigma} := \bar{\boldsymbol{\sigma}}$, etc.), while for ESP it employs variables ($\boldsymbol{\varepsilon} := \boldsymbol{\varepsilon}^*$, $\boldsymbol{\sigma} := \boldsymbol{\sigma}^*$, etc.) worked out later in this paper (Section 2.7).

The BSP model may be summarized as follows using a simplified notation. The state variables that define the problem are the composite internal variables ${}^f\boldsymbol{\varepsilon}, {}^m\boldsymbol{\varepsilon} \in \mathbf{Sym}, {}^f\boldsymbol{\beta} \in {}^fI, {}^m\boldsymbol{\beta} \in {}^mI$ plus the composite total strain $\boldsymbol{\varepsilon}$. The equations governing the problem are:

(1) the constitutive laws of both materials:

$$\begin{aligned} {}^c\dot{\boldsymbol{\sigma}} &= {}^c\boldsymbol{g}({}^c\boldsymbol{\varepsilon}, {}^c\boldsymbol{\beta}, {}^c\dot{\boldsymbol{\varepsilon}}), \\ {}^c\dot{\boldsymbol{\beta}} &= {}^c\boldsymbol{h}({}^c\boldsymbol{\varepsilon}, {}^c\boldsymbol{\beta}, {}^c\dot{\boldsymbol{\varepsilon}}) \end{aligned} \quad \text{with } c = f, m. \tag{16}$$

(2) the equation relating average strains and stresses:

$$\boldsymbol{\varepsilon} = {}^fk^f\boldsymbol{\varepsilon} + {}^mk^m\boldsymbol{\varepsilon}, \tag{17}$$

$$\boldsymbol{\sigma} = {}^fk^f\boldsymbol{\sigma} + {}^mk^m\boldsymbol{\sigma}. \tag{18}$$

(3) the BSP closure equations:

$${}^m\boldsymbol{\varepsilon}_{\mathrm{P}} = {}^f\boldsymbol{\varepsilon}_{\mathrm{P}}, \tag{19}$$

$${}^m\boldsymbol{\sigma}_{\mathrm{S}} = {}^f\boldsymbol{\sigma}_{\mathrm{S}}. \tag{20}$$

The algorithmic problem, regarded as a strain driven problem, may be stated as follows: "Given the state variables at time t:

$${}^t[{}^m\boldsymbol{\varepsilon}], {}^t[{}^m\boldsymbol{\varepsilon}], {}^t[{}^f\boldsymbol{\beta}], {}^t[{}^f\boldsymbol{\beta}], {}^t[\boldsymbol{\varepsilon}]$$

and the composite strain at time $t + \Delta t$:

$${}^{t+\Delta t}[\boldsymbol{\varepsilon}]$$

find the updated state of the composite at time $t + \Delta t$, defined by the set of variables:

$${}^{t+\Delta t}[{}^f\boldsymbol{\varepsilon}], {}^{t+\Delta t}[{}^m\boldsymbol{\varepsilon}], {}^{t+\Delta t}[{}^f\boldsymbol{\beta}], {}^{t+\Delta t}[{}^m\boldsymbol{\beta}], {}^{t+\Delta t}[\boldsymbol{\varepsilon}]$$

satisfying governing equations (16)–(20) in the interval $[t, t + \Delta t]$".

The next chart shows the known and unknown variables of the problem:

Known variables:	
${}^{t+\Delta t}[\boldsymbol{\varepsilon}]$,	free variable
${}^t[{}^m\boldsymbol{\varepsilon}], {}^t[{}^f\boldsymbol{\varepsilon}], {}^t[{}^m\boldsymbol{\beta}], {}^t[{}^f\boldsymbol{\beta}]$,	internal variables
Unknown variables:	
${}^{t+\Delta t}[{}^m\boldsymbol{\sigma}], {}^{t+\Delta t}[{}^f\boldsymbol{\sigma}], {}^{t+\Delta t}[\boldsymbol{\sigma}]$,	dependent variables
${}^{t+\Delta t}[{}^m\boldsymbol{\varepsilon}], {}^{t+\Delta t}[{}^f\boldsymbol{\varepsilon}], {}^{t+\Delta t}[{}^m\boldsymbol{\beta}], {}^{t+\Delta t}[{}^f\boldsymbol{\beta}]$,	updated internal variables

Variables ${}^m\boldsymbol{\beta}$ and ${}^f\boldsymbol{\beta}$ group together all the set of internal variables corresponding to the components, such as internal variables of damage and/or plasticity that define the state of the compounding materials: ${}^c\boldsymbol{\beta} := \{{}^c\boldsymbol{\varepsilon}^p, {}^c\mathbb{C}^d\}$.

In the following, it will be shown that the system of nonlinear equations defining the problem may be solved via a specifically devised Newton–Raphson iterative strategy.

The proposed algorithm is a general solver for composites that uses the constitutive models of component materials as 'black boxes'. This procedure allows one to use already-developed algorithms for homogeneous materials available in many FEM codes. This means that the algorithm for the local integration of the evolution equations is given for each component material:

$$\underbrace{\left\{{}^{t}\left[{}^{f}\boldsymbol{\varepsilon}\right],\ {}^{t}\left[{}^{f}\boldsymbol{\beta}\right]\right\}\ ;\ {}^{t+\Delta t}\left[{}^{f}\boldsymbol{\varepsilon}\right]}_{\Downarrow\ \text{Constitutive Algorithm for Fiber}\ \Downarrow}\quad \underbrace{\left\{{}^{t}\left[{}^{m}\boldsymbol{\varepsilon}\right],\ {}^{t}\left[{}^{m}\boldsymbol{\beta}\right]\right\}\ ;\ {}^{t+\Delta t}\left[{}^{m}\boldsymbol{\varepsilon}\right]}_{\Downarrow\ \text{Constitutive Algorithm for Matrix}\ \Downarrow}$$

$$\overbrace{{}^{t+\Delta t}\left[{}^{f}\boldsymbol{\beta}\right]\ ;\ {}^{t+\Delta t}\left[{}^{f}\boldsymbol{\sigma}\right]}\qquad \overbrace{{}^{t+\Delta t}\left[{}^{m}\boldsymbol{\beta}\right]\ ;\ {}^{t+\Delta t}\left[{}^{m}\boldsymbol{\sigma}\right]} \tag{21}$$

The solving algorithms for the constitutive laws of component materials will be denoted by 'fibre/matrix constitutive algorithms', while the algorithm for the resolution of the whole SP model will be denoted by 'composite algorithm'. Furthermore, each component material model must also provide the consistent tangent operator ${}^{c}\mathbb{C}$ for each component constitutive algorithm, sketched in (21). The composite algorithm will make use of the following serial–parallel decomposition of tangent operators:

$${}^{c}\mathbb{C} = \begin{bmatrix} \frac{\partial^{c}\boldsymbol{\sigma}_{\mathrm{P}}}{\partial^{c}\boldsymbol{\varepsilon}_{\mathrm{P}}} & \frac{\partial^{c}\boldsymbol{\sigma}_{\mathrm{P}}}{\partial^{c}\boldsymbol{\varepsilon}_{\mathrm{S}}} \\ \frac{\partial^{c}\boldsymbol{\sigma}_{\mathrm{S}}}{\partial^{c}\boldsymbol{\varepsilon}_{\mathrm{P}}} & \frac{\partial^{c}\boldsymbol{\sigma}_{\mathrm{S}}}{\partial^{c}\boldsymbol{\varepsilon}_{\mathrm{S}}} \end{bmatrix} = \begin{bmatrix} {}^{c}\mathbb{C}_{\mathrm{PP}} & {}^{c}\mathbb{C}_{\mathrm{PS}} \\ {}^{c}\mathbb{C}_{\mathrm{SP}} & {}^{c}\mathbb{C}_{\mathrm{SS}} \end{bmatrix},$$

$$\text{where}\quad \begin{cases} {}^{c}\mathbb{C}_{\mathrm{PP}} = \mathbb{P}_{\mathrm{P}} : {}^{c}\mathbb{C} : \mathbb{P}_{\mathrm{P}} \\ {}^{c}\mathbb{C}_{\mathrm{PS}} = \mathbb{P}_{\mathrm{P}} : {}^{c}\mathbb{C} : \mathbb{P}_{\mathrm{S}} \\ {}^{c}\mathbb{C}_{\mathrm{SP}} = \mathbb{P}_{\mathrm{S}} : {}^{c}\mathbb{C} : \mathbb{P}_{\mathrm{P}} \\ {}^{c}\mathbb{C}_{\mathrm{SS}} = \mathbb{P}_{\mathrm{S}} : {}^{c}\mathbb{C} : \mathbb{P}_{\mathrm{S}} \end{cases} \quad \text{with } c = m, f. \tag{22}$$

The serial part of matrix strain ${}^{m}\boldsymbol{\varepsilon}_{\mathrm{S}}$ is selected as the independent variable of the Newton–Raphson scheme to be adopted for the composite algorithm. The disequilibrium in the serial stresses $\Delta\boldsymbol{\sigma}_{\mathrm{S}}$ is taken as the residue to be zeroed by iterative solutions:

$$\Delta\boldsymbol{\sigma}_{\mathrm{S}} = {}^{m}\boldsymbol{\sigma}_{\mathrm{S}} - {}^{f}\boldsymbol{\sigma}_{\mathrm{S}}. \tag{23}$$

The total serial strain of one of the materials is chosen as the unknown – in this case the one from the matrix (${}^{m}\boldsymbol{\varepsilon}_{\mathrm{S}}$) – because the strain of the other material depends on the first one:

$${}^{f}\boldsymbol{\varepsilon}_{\mathrm{S}}({}^{m}\boldsymbol{\varepsilon}_{\mathrm{S}}) = \frac{1}{{}^{f}k}\boldsymbol{\varepsilon}_{\mathrm{S}} - \frac{{}^{m}k}{{}^{f}k}{}^{m}\boldsymbol{\varepsilon}_{\mathrm{S}}, \tag{24}$$

$$\Delta\boldsymbol{\sigma}_{\mathrm{S}}({}^{m}\boldsymbol{\varepsilon}_{\mathrm{S}}) = {}^{m}\boldsymbol{\sigma}_{\mathrm{S}}({}^{m}\boldsymbol{\varepsilon}_{\mathrm{S}}) - {}^{f}\boldsymbol{\sigma}_{\mathrm{S}}({}^{f}\boldsymbol{\varepsilon}_{\mathrm{S}}({}^{m}\boldsymbol{\varepsilon}_{\mathrm{S}})). \tag{25}$$

The derivative of the objective function (residue) with respect to the unknown:

$$\frac{\partial[\Delta\boldsymbol{\sigma}_{\mathrm{S}}]}{\partial^{m}\boldsymbol{\varepsilon}_{\mathrm{S}}} = \frac{\partial[{}^{m}\boldsymbol{\sigma}_{\mathrm{S}} - {}^{f}\boldsymbol{\sigma}_{\mathrm{S}}]}{\partial^{m}\boldsymbol{\varepsilon}_{\mathrm{S}}} = \frac{\partial^{m}\boldsymbol{\sigma}_{\mathrm{S}}}{\partial^{m}\boldsymbol{\varepsilon}_{\mathrm{S}}} - \frac{\partial^{f}\boldsymbol{\sigma}_{\mathrm{S}}}{\partial^{f}\boldsymbol{\varepsilon}_{\mathrm{S}}} : \frac{\partial^{f}\boldsymbol{\varepsilon}_{\mathrm{S}}}{\partial^{m}\boldsymbol{\varepsilon}_{\mathrm{S}}} \tag{26}$$

gives the expression of the Jacobian (in terms of component tangent operators):

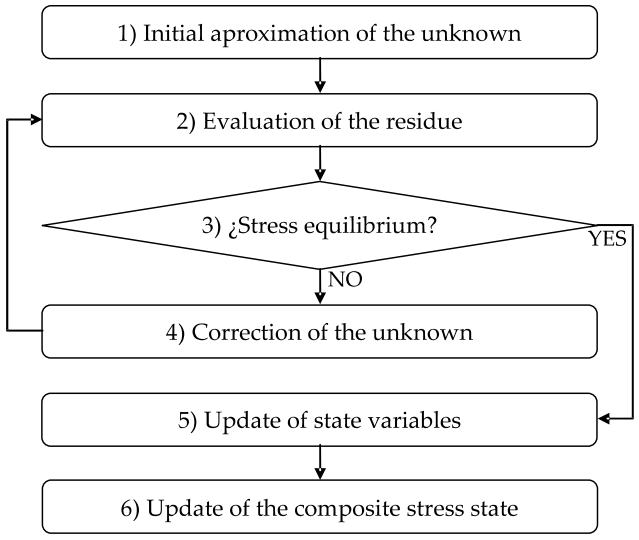

Fig. 1. Flow chart for the composite solving algorithm.

$$\begin{aligned} \mathbb{J}_{\kappa} = \left.\frac{\partial[\Delta\boldsymbol{\sigma}_{\mathrm{S}}]}{\partial^{m}\boldsymbol{\varepsilon}_{\mathrm{S}}}\right|_{{}^{m}\boldsymbol{\varepsilon}_{\mathrm{S}}=[{}^{m}\boldsymbol{\varepsilon}_{\mathrm{S}}]_{\kappa}} &= \frac{\partial[{}^{m}\boldsymbol{\sigma}_{\mathrm{S}}]_{\kappa}}{\partial^{m}\boldsymbol{\varepsilon}_{\mathrm{S}}} - \frac{\partial[{}^{f}\boldsymbol{\sigma}_{\mathrm{S}}]_{\kappa}}{\partial^{f}\boldsymbol{\varepsilon}_{\mathrm{S}}} : \frac{\partial^{f}\boldsymbol{\varepsilon}_{\mathrm{S}}}{\partial^{m}\boldsymbol{\varepsilon}_{\mathrm{S}}} \\ &= [{}^{m}\mathbb{C}_{\mathrm{SS}}]_{\kappa} - [{}^{f}\mathbb{C}_{\mathrm{SS}}]_{\kappa} : \left(-\frac{{}^{m}k}{{}^{f}k}\mathbb{I}\right) \\ &= [{}^{m}\mathbb{C}_{\mathrm{SS}}]_{\kappa} + \frac{{}^{m}k}{{}^{f}k}[{}^{f}\mathbb{C}_{\mathrm{SS}}]_{\kappa}, \end{aligned} \tag{27}$$

which is used to update the unknown at each local iterative step:

$$[{}^{m}\boldsymbol{\varepsilon}_{\mathrm{S}}]_{\kappa+1} = [{}^{m}\boldsymbol{\varepsilon}_{\mathrm{S}}]_{\kappa} - \mathbb{J}^{-1} : [\Delta\boldsymbol{\sigma}_{\mathrm{S}}]_{\kappa}. \tag{28}$$

The generic iteration of the Newton Raphson method will be denoted with the index κ. From now on and with no ambiguity, the trial quantities ${}^{t+\Delta t}[\bullet]_{\kappa}$ will be referred with $[\bullet]_{\kappa}$ in order to avoid a too complex notation.

Fig. 1 illustrates the flow chart of the composite solving algorithm to be implemented as a constitutive law in a FEM code. Each step of the algorithm will be briefly described in the following.

Step 1. Initial approximation.

The initial approximation of the unknown may be established by considering that the strain increment maintains the tangent evolution of the previous step.

First, the constitutive models of each material are evaluated to determine their constitutive tangent tensors corresponding to the previous step (time t).

$$\underbrace{{}^{t}\left[{}^{m}\boldsymbol{\varepsilon}\right]\ ;\ {}^{t}\left[{}^{m}\boldsymbol{\beta}\right]}_{\Downarrow\ \text{Matrix Model}\ \Downarrow}\qquad \underbrace{{}^{t}\left[{}^{f}\boldsymbol{\varepsilon}\right]\ ;\ {}^{t}\left[{}^{f}\boldsymbol{\beta}\right]}_{\Downarrow\ \text{Fibre Model}\ \Downarrow}$$

$$\overbrace{{}^{t}\left[{}^{m}\mathbf{C}\right]}\qquad \overbrace{{}^{t}\left[{}^{f}\mathbf{C}\right]}$$

Then, the increment of the unknown is determined, assuming that the total strain increment is distributed among constituent materials according to their previous step tangent stiffnesses:

$$
\begin{aligned}
&{}^{t}[\boldsymbol{\varepsilon}_S] = {}^{m}k^{t}[{}^{m}\boldsymbol{\varepsilon}_S] + {}^{f}k^{t}[{}^{f}\boldsymbol{\varepsilon}_S],\\
&[\Delta\boldsymbol{\varepsilon}_S] = {}^{t+\Delta t}[\boldsymbol{\varepsilon}_S] - {}^{t}[\boldsymbol{\varepsilon}_S],\\
&[\Delta\boldsymbol{\varepsilon}_P] = {}^{t+\Delta t}[\boldsymbol{\varepsilon}_P] - {}^{t}[{}^{m}\boldsymbol{\varepsilon}_P],\\
&[{}^{m}\Delta\boldsymbol{\varepsilon}_S]_0 = \mathbb{A} : [{}^{f}\mathbb{C}_{SS} : [\Delta\boldsymbol{\varepsilon}_S] + {}^{f}k({}^{f}\mathbb{C}_{SP} - {}^{m}\mathbb{C}_{SP}) : [\Delta\boldsymbol{\varepsilon}_P]],
\end{aligned}
$$

where $\mathbb{A} = ({}^{m}k^{f}\mathbb{C}_{SS} + {}^{f}k^{m}\mathbb{C}_{SS})^{-1}$.

Finally, the initial value of the unknown $[{}^{m}\boldsymbol{\varepsilon}_S]_\kappa$ is established.

$$
\begin{aligned}
&[{}^{m}\boldsymbol{\varepsilon}_S]_\kappa = {}^{t}[{}^{m}\boldsymbol{\varepsilon}_S] + [{}^{m}\Delta\boldsymbol{\varepsilon}_S]_0,\\
&\kappa = 0.
\end{aligned}
$$

Step 2. Residue evaluation.

The total strain tensors of the components ($[{}^{m}\boldsymbol{\varepsilon}]_\kappa$ and $[{}^{f}\boldsymbol{\varepsilon}]_\kappa$) are determined as a function of the updated value of $[{}^{m}\boldsymbol{\varepsilon}_S]_\kappa$.

$$
\begin{aligned}
&[{}^{m}\boldsymbol{\varepsilon}]_\kappa = [{}^{m}\boldsymbol{\varepsilon}_P] + [{}^{m}\boldsymbol{\varepsilon}_S]_\kappa, \quad \text{where } [{}^{m}\boldsymbol{\varepsilon}_P] = [{}^{f}\boldsymbol{\varepsilon}_P] = {}^{t+\Delta t}[\boldsymbol{\varepsilon}_P],\\
&[{}^{f}\boldsymbol{\varepsilon}]_\kappa = [{}^{f}\boldsymbol{\varepsilon}_P] + [{}^{f}\boldsymbol{\varepsilon}_S]_\kappa, \quad \text{where } [{}^{f}\boldsymbol{\varepsilon}_S]_\kappa = \frac{1}{{}^{f}k}{}^{t+\Delta t}[\boldsymbol{\varepsilon}_S] - \frac{{}^{m}k}{{}^{f}k}[{}^{m}\boldsymbol{\varepsilon}_S]_\kappa.
\end{aligned}
$$

The constitutive models of each material are checked to determine their updated internal variables and stress states.

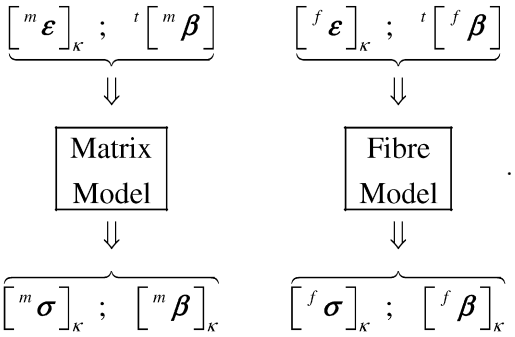

Thereafter, the residue is evaluated to find out whether the stress equilibrium (i.e., the convergence of the model) has been achieved.

$$
\begin{aligned}
[\Delta\boldsymbol{\sigma}_S]_\kappa = [{}^{m}\boldsymbol{\sigma}_S]_\kappa - [{}^{f}\boldsymbol{\sigma}_S]_\kappa \quad \text{where} \quad & [{}^{m}\boldsymbol{\sigma}_S]_\kappa = \mathbb{P}_S : [{}^{m}\boldsymbol{\sigma}]_\kappa,\\
& [{}^{f}\boldsymbol{\sigma}_S]_\kappa = \mathbb{P}_S : [{}^{f}\boldsymbol{\sigma}]_\kappa.
\end{aligned}
$$

Step 3. Convergence checking.

In order to choose the tolerance, the order of magnitude of the serial stresses should be considered as a reference. If the stresses of the previous step are different from zero, the minimum between them is taken; otherwise, the linearized stresses are taken as a reference.

$$
\begin{aligned}
&\text{ref1} = \min\{\|{}^{t}[{}^{m}\boldsymbol{\sigma}_S]\|, \|{}^{t}[{}^{f}\boldsymbol{\sigma}_S]\|\},\\
&\text{ref2} = \min\{\|{}^{t}[{}^{m}\mathbb{C}_{SS}] : [\boldsymbol{\varepsilon}_S]\|, \|{}^{t}[{}^{f}\mathbb{C}_{SS}] : [\boldsymbol{\varepsilon}_S]\|\},\\
&\text{If} \quad \text{ref1} > 0 \quad \text{then :} \quad \text{refer} = \text{ref1},\\
&\qquad\qquad\quad \text{else :} \quad \text{refer} = \text{ref2}.
\end{aligned}
$$

The tolerance is chosen according to the reference value:

$$\text{toler} = \text{refer} \cdot 10^{-4}.$$

If the norm of the residue is greater than the tolerance, then go to step 4 – correction of the unknown, otherwise go to step 5 – update of variables.

$$
\begin{aligned}
&\text{If} \quad \|[\Delta\boldsymbol{\sigma}_S]_\kappa\| > \text{toler} \quad \text{then :} \quad \text{goto Step 4},\\
&\qquad\qquad\qquad\qquad\quad \text{else :} \quad \text{goto Step 5}.
\end{aligned}
$$

Step 4. Correction of the unknown.

(a) Evaluation of tangent constitutive tensors of both materials.The constitutive models of each material are evaluated to determine their tangent constitutive tensors.

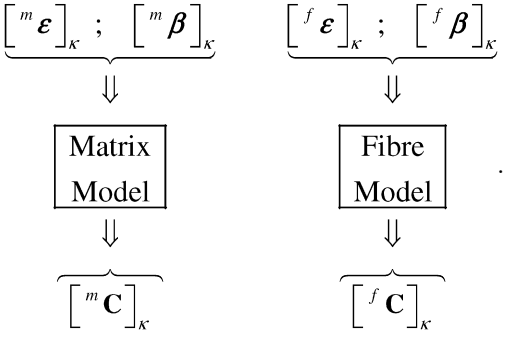

(b) Calculation of the Jacobian.

$$
[\mathbb{J}]_\kappa = [{}^{m}\mathbb{C}_{SS}]_\kappa + \tfrac{{}^{m}k}{{}^{f}k}[{}^{f}\mathbb{C}_{SS}]_\kappa \quad \text{where} \quad
\begin{aligned}
&[{}^{m}\mathbb{C}_{SS}]_\kappa = \mathbb{P}_S : [{}^{m}\mathbb{C}]_\kappa : \mathbb{P}_S,\\
&[{}^{f}\mathbb{C}_{SS}]_\kappa = \mathbb{P}_S : [{}^{f}\mathbb{C}]_\kappa : \mathbb{P}_S.
\end{aligned}
$$

(c) Update of the unknown.

$$
\begin{aligned}
&[{}^{m}\boldsymbol{\varepsilon}_S]_\kappa := [{}^{m}\boldsymbol{\varepsilon}_S]_\kappa - [\mathbb{J}]_\kappa^{-1} : [\Delta\boldsymbol{\sigma}_S]_\kappa,\\
&\kappa := \kappa + 1.
\end{aligned}
$$

Go to step 2 – residue evaluation.

Step 5. Update of variables.

Once the convergence of the constitutive model has been obtained, all the variables of the model must be updated:

$$
\begin{aligned}
&{}^{t+\Delta t}[{}^{m}\boldsymbol{\varepsilon}_S] = [{}^{m}\boldsymbol{\varepsilon}_S]_\kappa; \quad {}^{t+\Delta t}[{}^{m}\boldsymbol{\beta}] = [{}^{m}\boldsymbol{\beta}]_\kappa; \quad {}^{t+\Delta t}[{}^{m}\boldsymbol{\sigma}] = [{}^{m}\boldsymbol{\sigma}]_\kappa,\\
&{}^{t+\Delta t}[{}^{f}\boldsymbol{\varepsilon}_S] = [{}^{f}\boldsymbol{\varepsilon}_S]_\kappa; \quad {}^{t+\Delta t}[{}^{f}\boldsymbol{\beta}] = [{}^{f}\boldsymbol{\beta}]_\kappa; \quad {}^{t+\Delta t}[{}^{f}\boldsymbol{\sigma}] = [{}^{f}\boldsymbol{\sigma}]_\kappa.
\end{aligned}
$$

Step 6. Update of the composite stress state.

The stress tensor of the composite is calculated by taking into account Eq. (18):

$${}^{t+\Delta t}[\boldsymbol{\sigma}] = {}^{m}k^{t+\Delta t}[{}^{m}\boldsymbol{\sigma}] + {}^{f}k^{t+\Delta t}[{}^{f}\boldsymbol{\sigma}].$$

The presented algorithm manages to compound the behaviours of materials, fulfilling the governing equations of the basic serial–parallel problem.

2.6. Tangent operator of the BSP model

In addition to the solving algorithm for the composite model, the solution of the global problem also requires

the calculation of the tangent operator. If the global problem is solved via the finite element method, for example, this operation must be accomplished when assembling the elemental stiffness matrix.

The derivation of the tangent matrix for the composite is performed by linearizing the equations governing the BSP model. Its deduction is detailed in the Annex of this work.

Making use of the decomposition form (22), the composite tangent operator is given by

$$\boxed{\mathbb{C} = \begin{bmatrix} \frac{\partial \boldsymbol{\sigma}_P}{\partial \boldsymbol{\varepsilon}_P} & \frac{\partial \boldsymbol{\sigma}_P}{\partial \boldsymbol{\varepsilon}_S} \\ \frac{\partial \boldsymbol{\sigma}_S}{\partial \boldsymbol{\varepsilon}_P} & \frac{\partial \boldsymbol{\sigma}_S}{\partial \boldsymbol{\varepsilon}_S} \end{bmatrix} = \begin{bmatrix} \mathbb{C}_{PP} & \mathbb{C}_{PS} \\ \mathbb{C}_{SP} & \mathbb{C}_{SS} \end{bmatrix},}$$

where

$$\boxed{\begin{aligned} &\mathbb{C}_{PP} = ({}^f k^f \mathbb{C}_{PP} + {}^m k^m \mathbb{C}_{PP}) + {}^m k^f k({}^f \mathbb{C}_{PS} - {}^m \mathbb{C}_{PS}) : \mathbb{A} : ({}^m \mathbb{C}_{SP} - {}^f \mathbb{C}_{SP}), \\ &\mathbb{C}_{PS} = ({}^f k^f \mathbb{C}_{PS} : \mathbb{A} : {}^m \mathbb{C}_{SS} + {}^m k^m \mathbb{C}_{PS} : \mathbb{A} : {}^f \mathbb{C}_{SS}), \\ &\mathbb{C}_{SP} = ({}^m k^f \mathbb{C}_{SS} : \mathbb{A} : {}^m \mathbb{C}_{SP} + {}^f k^m \mathbb{C}_{SS} : \mathbb{A} : {}^f \mathbb{C}_{SP}), \\ &\mathbb{C}_{SS} = \tfrac{1}{2}[({}^m \mathbb{C}_{SS} : \mathbb{A} : {}^f \mathbb{C}_{SS}) + ({}^f \mathbb{C}_{SS} : \mathbb{A} : {}^m \mathbb{C}_{SS})] \end{aligned}} \tag{29}$$

and

$$\mathbb{A} = ({}^f k^m \mathbb{C}_{SS} + {}^m k^f \mathbb{C}_{SS})^{-1}. \tag{30}$$

It is worth noting that the composite tangent operator is symmetric when the tangent operators of component materials are also symmetric. Indeed, if ${}^f\mathbb{C}$ and ${}^m\mathbb{C}$ are symmetric then:

$${}^c\mathbb{C}_{SS} = {}^c\mathbb{C}_{SS}^T, \quad {}^c\mathbb{C}_{SP} = {}^c\mathbb{C}_{PS}^T, \quad \text{with } c = m, f.$$

With these properties, expressions (29) imply: $\mathbb{C}_{SS} = \mathbb{C}_{SS}^T$, $\mathbb{C}_{SP} = \mathbb{C}_{PS}^T$, $\mathbb{C}_{PP} = \mathbb{C}_{PP}^T$, as the reader would easily check.

2.7. The enriched SP model

It was pointed out in Section 2.4 that the isostress assumption in orthogonal directions to the fibre (pure serial behaviour in transverse directions) constitutes a lower bound for the transverse/shear stiffness of the composite, and for this reason the BSP model needs to be enriched in order to predict the transversal/shear behaviour more accurately.

To avoid using a more complex model, and since the governing equations for the ESP model maintain the structure of the governing equations for the BSP model (16)–(20), the new solving algorithm is similar to the one developed in Section 2.5. The only difference is the use of $({}^m\boldsymbol{\varepsilon})^*$, $({}^m\boldsymbol{\sigma})^*$, $({}^m\mathbb{C})^*$ instead of ${}^m\boldsymbol{\varepsilon}$, ${}^m\boldsymbol{\sigma}$, ${}^m\mathbb{C}$, whose expressions involve different close equations to provide a better account for the internal morphology of the composite, and for the stress/strain concentration in the matrix:

$$({}^m\boldsymbol{\varepsilon})^* = [{}^m\mathbb{K}]^{-1} : {}^m\boldsymbol{\varepsilon}, \tag{31}$$

$$({}^m\boldsymbol{\sigma})^* = {}^m\mathbb{K} : {}^m\boldsymbol{\sigma}, \tag{32}$$

$$({}^m\mathbb{C})^* = {}^m\mathbb{K} : {}^m\mathbb{C} : {}^m\mathbb{K}, \tag{33}$$

where ${}^m\mathbb{K} = \mathbb{P}_P : \mathbb{I} : \mathbb{P}_P + {}^m\gamma\mathbb{P}_S : \mathbb{I} : \mathbb{P}_S$.

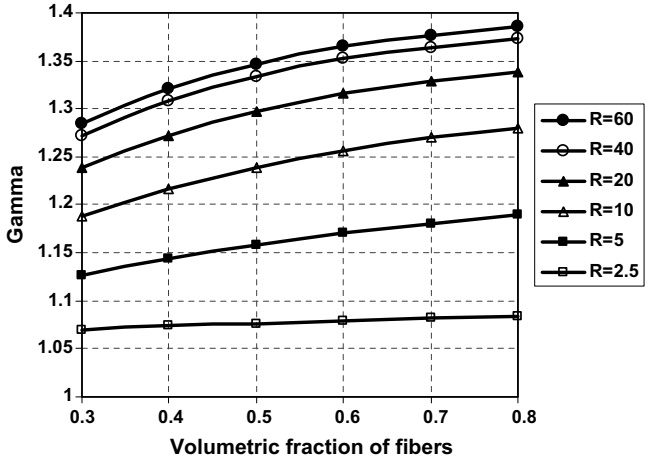

Fig. 2. Set of curves to estimate gamma values in terms of the fibre volume fraction and fibre/matrix stiffness ratio.

It is worth noting here that ${}^f\gamma = 1$, since the fibre stress remains uniform, and consequently it is not necessary to perform a change of variables for fibre material.

The gamma parameter ${}^m\gamma$ may be obtained through experimental calibration with lamina tests data, or through analytical analysis.

By means of micro-mechanical considerations described in [1], it is possible to adopt values of the gamma parameter ${}^m\gamma$ in terms of the fibre volume fraction (${}^f k$) and the ratio between fibre and matrix Young modules ($R = {}^f E/{}^m E$).

The following analytical expression for the parameter ${}^m\gamma$ is proposed:

$$\boxed{{}^m\gamma = \frac{\sqrt{\eta + \omega^2(1-\eta)}}{\eta + \omega(1-\eta)},} \tag{34}$$

$$\boxed{\text{where} \quad \omega = 1 + (R-1)\sqrt{{}^f k} \text{ and } \eta = \tfrac{\sqrt{{}^f k}}{1+{}^f k}.}$$

Fig. 2 shows a set of curves that have been obtained by means of the formula (34), which allow quick adoption of values for the gamma parameter to represent the composite transverse and shear stiffness better, e.g. ${}^m\gamma = 1.31$ for $R = 20$ and ${}^f k = 0.6$.

It will be shown in the validation section that the basic SP model, as well as inverse ROM, underestimates the experimental values, while the enriched SP model obtains an approximation to experimental data as good as the one given by the Halpin–Tsai equation.

Nevertheless, the Halpin–Tsai equation is restricted to the linear elastic region, while the ESP model also provides answers for the non-linear behaviour of the composite material.

3. Validation and calibration

The purpose of this section is to show and discuss the results of several numerical analyses devised to validate the response of the proposed model (in its two versions:

BSP and ESP), concerning both accuracy and computational cost.

Since the proposed model is based on the proper management of the component constitutive models, it is essential to adopt the specific constitutive laws that better represent the mechanical behaviour of each component phase, in each particular analysis. When the general response of the model is studied, fictitious materials are used in order to be able to better appreciate the interaction between component phases. This also allows one to check the capability of the model to 'compound' diverse constitutive behaviours. Both damage and plasticity models are used, with hardening and softening laws. On the other hand, when the objective is to reproduce as accurately as possible the mechanical response of real composite materials, a non-iso-resistent damage constitutive law is selected for both fibre and matrix. The conducted calibration procedure is then detailed.

The performed tests may be divided in two groups: group (a) tests for general validation of the model carried out on a unidirectional lamina, and group (b) tests to assess the predictive capability against experimental data. Among the validations of the first group, there are numerical simulations devised to investigate the fulfilment of the closure equation, the general behaviour of the model, the response given for stiffness and for strength, and the computational performance. The validations of the latter group are taken instead from the "world-wide failure exercise" [2], which is considered to be a reliable and complete set of benchmark test cases.

Since the response is verified 'locally', the validations are performed on an isoparametric hexahedral finite element with a laminated structure whenever required. On each ply of the laminate, the proposed composite model is used as the constitutive law. The term "hexahedral composite element" will be used to refer to this finite element in which the proposed composite model is used as the constitutive material model in its layer integration points.

3.1. Close equations fulfilment

In this section, the fulfilment of the close equations is verified as part of the validation process. With this aim in mind, stress and strain states are analysed not only in components phases but also in the composite material. The unidirectional lamina under study is subjected to two loading scenarios, named "parallel loading" and "transversal loading", where the applied loads are parallel or perpendicular to fibre direction, respectively.

It is worth noting that the constitutive model permanently fulfils all close equations independently of the loading scenario. These particular loading cases were chosen as validation and study samples, but of course, the composite material may also be subjected to bi- or tri-axial loading.

In the following numerical testing, the mechanical properties of matrix and fibre are chosen in order to make the main features of the model clearly detectable. They do not correspond to real materials, and for this reason are called material 'M' and material 'F', respectively.

3.1.1. Parallel loading

To test the proposed constitutive model under parallel loading, a load–unload controlled longitudinal deformation in fibre direction is applied to a hexahedral finite element with no other constrains. The mechanical properties of component materials are shown in Table 1.

Fig. 3 shows the response obtained for parallel strain ε_P vs. parallel stress σ_P. By virtue of the compatibility

Table 1
Mechanical properties of constituents selected for parallel loading test

	Material 'M'	Material 'F'
Constitutive law	J2 perfect plasticity	J2 perfect plasticity
Young modulus (MPa)	40 000	80 000
Elastic limit (MPa)	1000	3480
Poisson ratio	0.0	0.0
Volume fraction	0.58	0.42

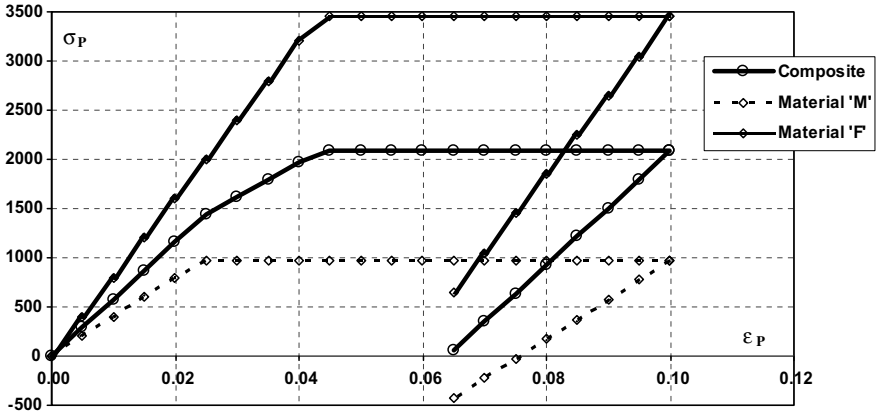

Fig. 3. Parallel stress (MPa) vs. parallel strain curves for the composite and component materials under parallel deformation-controlled load–unload testing.

equation, parallel strain is equal throughout the whole process in both fibre and matrix as well as in the composite. In the first elastic branch, perfect R.O.M. stiffness is obtained for the composite. Composite stiffness is then reduced when the matrix yields. Composite perfect plasticity is achieved after the fibre reaches its yielding limit. Loading is reversed at 10% strain. Initial elastic stiffness is shown in all materials during unloading. At complete unload, residual stresses remain in the components due to plasticity. These residual stresses are auto-equilibrated since the resultant stress in the composite is zero.

3.1.2. Transversal loading

In order to validate the serial behaviour of the model, a hexahedral composite element is subjected to pure transversal loading. The test is performed by applying a load–unload transversal controlled deformation up to 5% strain. No other constrains are set. The constitutive law selected for the material 'F' is an isotropic damage model with softening, while for the material 'M', a J2 plasticity model with exponential hardening is chosen. The main mechanical properties of these materials are shown in Table 2.

Note that Poisson ratios are set equal to zero, in order to avoid "coupling" with longitudinal behaviour, which is not desirable at this stage of the validation process. It will be further seen that the model can also deal with different Poisson ratios. Note also that material 'M' is softer and has a lower elastic limit than material 'F'.

Table 2
Mechanical properties of constituents selected for testing the SP model under transversal loading (serial behaviour)

	Material 'F'	Material 'M'
Constitutive law	Iso-damage with softening	J2 plasticity with hardening
Young modulus (MPa)	3000	2000
Elastic limit (MPa)	60	40
Poisson ratio	0.0	0.0
Volume fraction	0.5	0.5

In Fig. 4, the transversal stresses σ_S observed in all materials during the validation process are plotted against their respective transversal strains ε_S. The simulation shows that at each step of the analysis the closure equation is exactly fulfilled; this is denoted by the fact that at each step the serial stresses are identical for all materials. In the first elastic branch (O-A), the composite transversal stiffness, given by SP model, is in accordance with the inverse ROM. When material 'M' reaches the yielding threshold – point (A) in the composite – this material experiments plastic deformations, but keeps on incrementing its stress due to its hardening law. This fact also brings about a reduction in the composite stiffness along the branch (A–B), while material 'F' remains elastic up to point (B), when its damage begins. Material 'F' damages along branch (B–C), and thus causes all stresses to decrease; as a consequence, material 'M' experiments elastic unload. From point (C) on, the sign of the applied deformation is reversed (unloading), consequently all materials experiment elastic unload. Note that the material 'F' unloads with a reduced stiffness due to internal damage. Note also that the material 'M' unloads with the virgin elastic stiffness, and at complete unload retains residual plastic strains.

3.1.3. Remark

The fulfilment of close equations is verified not only in the linear-elastic region but also in the material non-linear behaviour, including the softening process for all loading scenarios applied.

3.2. Stiffness validations

The composite stiffness provided by the numerical model is studied for off-axis loading. Moreover, the

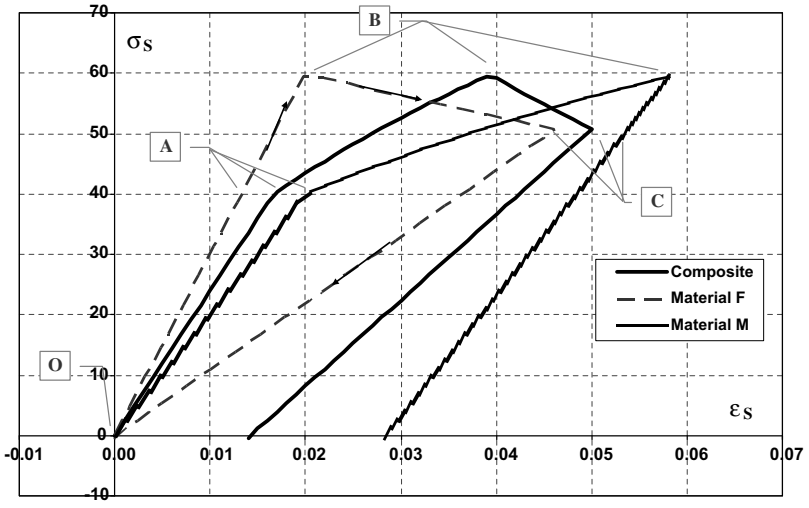

Fig. 4. Serial stress (MPa) vs. serial strain curves for the composite and component materials under transversal deformation-controlled load–unload testing.

influence of fibre volume fraction over longitudinal, transverse and in-plane shear stiffnesses is also analysed.

3.2.1. Off-axis stiffness

In this validation an hexahedral finite element composed of two isotropic elastic materials is subjected to uniaxial stress (force-controlled loading) applied in several directions, rotated by an angle θ with respect to fibre direction. The mechanical properties of these materials are shown in Table 3.

The SP model provides the following stiffness matrix in local fibre direction $C_{\theta=0}$ from which compliance matrix D may be also evaluated.

$$C_{\theta=0} = \begin{pmatrix} 71827 & 12452 & 12452 & 0 & 0 & 0 \\ 12452 & 31461 & 18102 & 0 & 0 & 0 \\ 12452 & 18102 & 31461 & 0 & 0 & 0 \\ 0 & 0 & 0 & 6679 & 0 & 0 \\ 0 & 0 & 0 & 0 & 6679 & 0 \\ 0 & 0 & 0 & 0 & 0 & 6679 \end{pmatrix} \cdot \text{MPa}$$

$$\Rightarrow \quad D = (C_{\theta=0})^{-1},$$

$$D = \begin{pmatrix} 15.251 & -3.832 & -3.832 & 0 & 0 & 0 \\ -3.832 & 48.480 & -26.378 & 0 & 0 & 0 \\ -3.832 & -26.378 & 48.480 & 0 & 0 & 0 \\ 0 & 0 & 0 & 149.714 & 0 & 0 \\ 0 & 0 & 0 & 0 & 149.714 & 0 \\ 0 & 0 & 0 & 0 & 0 & 149.714 \end{pmatrix} \cdot 10^{-6}\ \text{MPa}^{-1}.$$

Table 3
Mechanical properties of constituents adopted to validate off-axis stiffness

	Fibre	Matrix
Material	Glass	Epoxy
Young modulus (MPa)	105950	5000
Poisson ratio	0.22	0.38
Volume fraction	0.6	0.4

As shown in Fig. 5, the curve obtained by plotting the resulting stiffness vs. the angle θ coincides exactly with the curve given by coordinate transformation of material compliance coefficients formulas (see [23, p. 98]):

$$\frac{1}{E_\theta} = D_{11}\cos^4\theta - 2D_{16}\cos^3\theta\sin\theta + (2D_{12}+D_{66})\cos^2\theta\sin^2\theta - 2D_{26}\cos\theta\sin^3\theta + D_{22}\sin^4\theta,$$

where D_{ij} indicates the coefficients of the compliance matrix.

3.2.2. Longitudinal stiffness vs. fibre volume fraction

The component materials from the previous validation are taken to study the influence of different fibre volume fraction in the longitudinal stiffness of long fibre composites (LFC). The longitudinal stiffness E_1 is obtained with the BSP and ESP model for several fibre volume fractions V_f. As expected, the model exactly reproduces a ROM prediction in the parallel direction, presenting linear variation in terms of V_f between 5000 MPa (for $V_f = 0$) and 105950 Mpa (for $V_f = 1$) that are matrix and fibre Young modulus, respectively.

3.2.3. Transversal stiffness vs. fibre volume fraction

In this validation, the predictive capacity of BSP and ESP models for the transversal stiffness of a glass–epoxy laminate with $E_F/E_M = 21.19$, $v_F = 0.22$, $v_M = 0.38$ (the same component materials specified in Table 3) is compared against experimental data and against the approximation given by broadly used semi-empirical formulas. The validation consists in subjecting a hexahedral composite element to pure transversal loading at different fibre volume fractions V_f.

In Fig. 6, the adimensional curves E_f/E_m vs. V_f resulting from basic SP and Enriched SP simulations are reported together with experimental values taken from Barbero

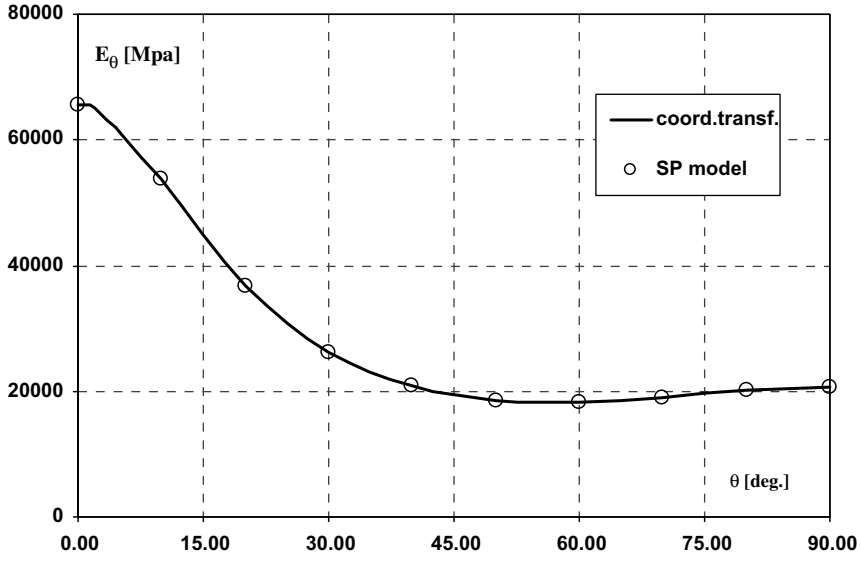

Fig. 5. Off-axis stiffness (MPa) curve for the composite.

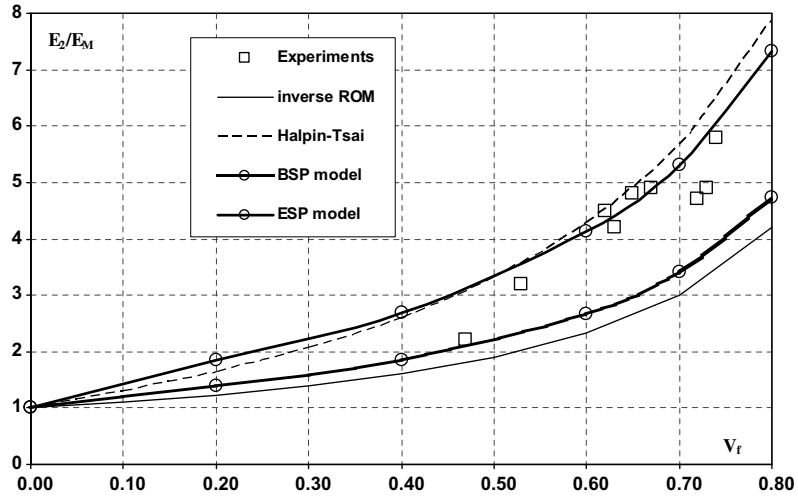

Fig. 6. Relative transversal stiffness E_2/E_M vs. fibre volume fraction V_f. Comparison between the results given by the proposed models, experimental data, inverse ROM and Halpin–Tsai equation.

[24, p. 72]. In the same figure, the curves resulting from perfect inverse ROM and from Halpin–Tsai equation [25] are also provided for comparison:

$$\frac{E_2}{E_M} = \frac{1 + \xi\eta V_F}{1 - \eta V_F} \quad \text{with } \eta = \frac{\left(\frac{E_F}{E_M}\right) - 1}{\left(\frac{E_F}{E_M}\right) + \xi},$$

in which the coefficient ξ is set equal to 2, the usual suggested value for circular fibres in a square array – see [26,24].

The transversal stiffness obtained by the simple SP model turns out to be slightly greater than the one given by inverse ROM, due to Poisson effects (fibre longitudinal constrain). Obviously, when Poisson ratios are set equal to zero a perfect inverse ROM curve is recovered. The graph shows that the simple SP model and the inverse ROM appreciably underestimate the experimental values (an already well established fact for the latter). On the other hand, the Enriched SP model, with the adopted gamma evaluation, gives an approximation to experimental data as good as the one given by Halpin–Tsai equation, which is one of the formulae most frequently employed when only limited experimental information is available. It is important to remark that in the ESP model no experimental coefficient was introduced to fit experimental data, since this model is based only on micro-mechanical considerations.

All previous validations, which, for sake of simplicity, are illustrated only for the Basic SP model, are also fulfilled by the ESP model.

3.2.4. In-plane shear stiffness vs. fibre volume fraction

In this validation, the predictive capacity of SP and ESP models for in-plane shear stiffness of a glass–epoxy laminate with $G_F/G_M = 20.0$ is compared against experimental data and against the approximation given by the Halpin–Tsai equation.

Table 4
Mechanical properties of constituents adopted to validate in-plane shear stiffness

	Fibre	Matrix
Material	E-glass	Epoxy
Young modulus (MPa)	72300	4000
Poisson ratio	0.22	0.35
Shear modulus (MPa)	29631	1481

Table 4 specifies the mechanical properties of component materials.

The validation consists in subjecting a hexahedral composite element to in-plane shear loading, at different fibre volume fractions. In Fig. 7, the adimensional curves G_F/G_M vs. V_F resulting from SP and ESP simulations are reported together with experimental values taken from Barbero [24, p. 75]. In the same figure, the curve resulting from perfect inverse ROM and that obtained from the Halpin–Tsai equation are also reported. In this case the value adopted for coefficient ξ is 1, as suggested by Halpin–Tsai [25].

Since for shear there is no coupling (i.e. fibre longitudinal constrain does not affect shearing), the transversal stiffness exhibited by the BSP model coincides with that given by the inverse ROM. In any case, the graph shows that this is a simple although inaccurate prediction of the in-plane shear modulus. The ESP model provides a better approximation to experimental data, which turns out to be as good as the one given by the Halpin–Tsai equation.

3.3. Off-axis strength validation

In this validation an hexahedral composite element, composed of the same materials used in previous strength validations for carbon–epoxy laminates and with

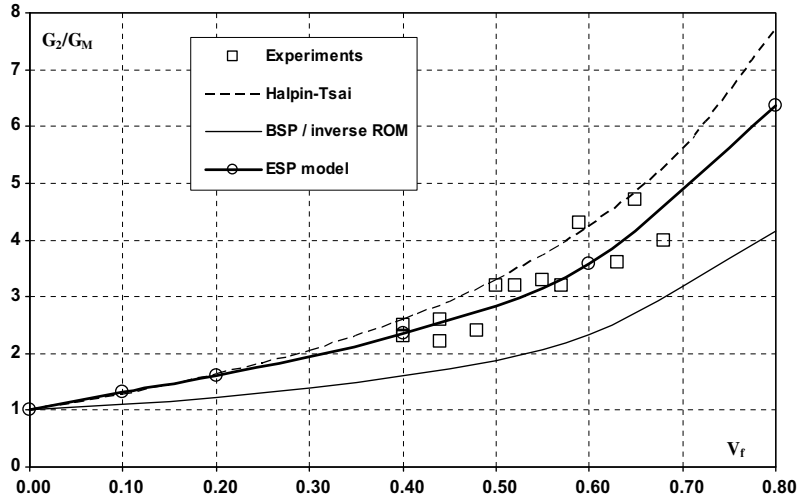

Fig. 7. Relative shear stiffness G_{12}/G_M vs. fibre volume fraction V_f. Comparison between experimental data, inverse ROM, Halpin–Tsai equation and results given by BSP and ESP models.

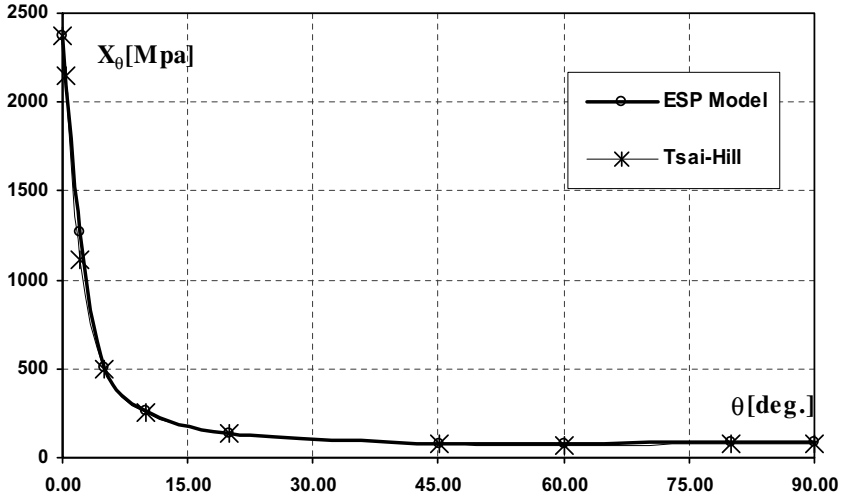

Fig. 8. Off-axis strength (MPa) curve for a carbon–epoxy unidirectional lamina subjected to force-controlled loading applied at different angles.

$V_f = 0.60$, is subjected to uniaxial stress (i.e. force-controlled loading) applied in a direction rotated by an angle θ with respect to fibre direction. The ultimate strength given by the proposed model in function of the angle θ is shown in Fig. 8.

The curve obtained by the ESP model almost exactly superposes the one corresponding to the Tsai–Hill criterion – see [24], given by

$$X_{\theta TH} = \frac{1}{\sqrt{\frac{\cos^4\theta}{X_1^2} + \frac{\sin^4\theta}{X_2^2} - \frac{\sin^2\theta\cos^2\theta}{X_1^2} + \frac{\sin^2\theta\cos^2\theta}{X_{12}^2}}}.$$

Only for very small angles, the curve presents a non-smooth shape which makes it more similar to the maximum stress criterion. This is due to the fact that the SP model naturally distinguishes between fibre failure and matrix failure (see Fig. 9).

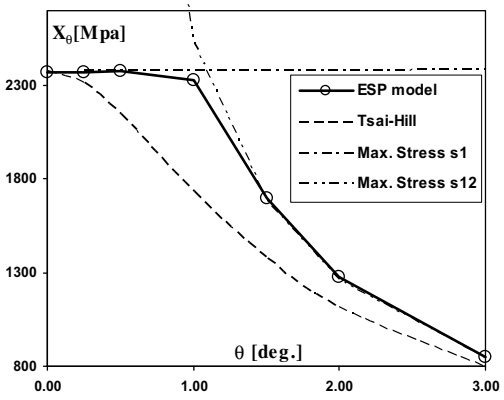

Fig. 9. Detail of the ultimate composite strength (MPa) curve at very low off-axis angles for a carbon–epoxy unidirectional lamina. Comparison with Tsai–Hill and maximum-stress criteria.

3.4. Calibration procedure for component materials

3.4.1. Preliminary considerations

Before proceeding to the calibration of component materials properties against experimental data, it is worth taking some preliminary considerations into account. Not all of the mechanical properties of the lamina may be predicted by merely using the properties of the isolated component materials. This fact is indeed also noted by other authors such as Puck and Schürmann [4]. Actually, the calibration also depends on the constitutive models selected for the component materials. The presence of an epoxy or metal matrix, for example, requires different constitutive laws and, consequently, different calibration procedures. For the particular case of fibre-reinforced plastics, an important characteristic required by the component models is that they must not be iso-resistant. For the matrix this is a well-known fact due to the usual presence of microvoids.

In the case of the fibres, different tensile and compressive strength thresholds are needed to account for the phenomenon of micro-buckling, in lieu of a more appropriate model. With this in view, the constitutive model adopted to simulate the behaviour of the both component materials for the present calibration procedure is a standard isotropic damage model with two different damage variables for tension and compression d^+/d^- (see [27] for details).

In the following, the calibration is carried out for the E-glass/epoxy LY556 considered in the world-wide failure exercise (WWFE) [2], whose properties are reported by Soden et al. [28]. Data given for the WWFE are the lamina stiffness and strength, and components mechanical properties. Using these data, participants in the WWFE were asked to provide the failure envelope for lamina and laminate. The material resulting from this calibration will be subsequently tested against the experimental data provided by Soden et al. [29].

3.4.2. Stiffness parameters

The stiffness parameters for matrix and fibre are set equal to the values provided for isolated materials (see Table 5).

3.4.3. Strength parameters for the matrix

Matrix compressive and tensile strengths are set equal to the corresponding transverse strengths exhibited by the unidirectional lamina: $X_{mT} = 40$ MPa, $X_{mC} = 135$ MPa. Note that the values adopted are those given by Hütter et al. [30], whose experimental results were taken as reference for the "failure exercise". These experimental data do not exactly agree with the strength values formerly provided by Soden et al. [28].

Table 5
Stiffness parameters adopted for component materials of LY556 glass–epoxy laminas

Stiffness properties	Matrix	Fibre
Young modulus (MPa)	3350	80000
Poisson ratio	0.35	0.20

3.4.4. Strength parameters for the fibre

To calibrate tensile and compressive strength of fibres, it is not convenient to consider them isolated, but inside the lamina. Thus, the quota of lamina strength attributed to fibres is worked out:

$$X_{fT} = \frac{X_T - \sigma_{mT} V_m}{V_f}, \quad X_{fC} = \frac{X_C - \sigma_{mC} V_m}{V_f},$$

where σ_{mT} and σ_{mC} are, respectively, the stress in the matrix in correspondence with lamina ultimate longitudinal tensile and compressive strength.

Moreover, extra considerations may be taken into account according to each case.

For compressive strength, matrix may be considered to remain elastic when lamina fails, so that we may infer:

$$\sigma_{mC} = \frac{E_m}{E_f} X_{fC}.$$

This leads to the following formula:

$$X_{fC} = \frac{X_C}{V_f + V_m \frac{E_m}{E_f}} = \frac{570}{0.62 + 0.38 \frac{3.35}{80}} = 896 \text{ MPa}.$$

For the calibration of longitudinal tensile strength in a GFRP, it is assumed that in correspondence to fibre ultimate tensile strength, matrix has already failed and thus its contribution to lamina strength is negligible. This assumption leads to:

$$X_{fT} = \frac{X_T}{V_f} = \frac{1140}{0.62} = 1839 \text{ MPa}.$$

3.4.5. Summary of calibrated properties

The complete list of material properties adopted for LY556 unidirectional lamina are summarised in Table 6.

Post-failure behaviour has to be calibrated by the appropriate election of fracture energies for matrix and fibre, in order to match stress–strain curves of lamina provided by the experimental tests.

3.4.6. Remark

It is worth noting that the fibre local buckling phenomenon is taken into account by reducing the fibre strength at

Table 6
Calibrated properties for component materials of LY556 glass–epoxy laminas

Mechanical properties	Fibre	Matrix
Material	E-glass	Epoxy
Constitutive law	Damage d+/d−	Damage d+/d−
Young modulus (MPa)	80000	3350
Poisson ratio	0.20	0.35
Tensile strength (MPa)	1839	40
Compressive strength (MPa)	896	135
Volume fraction	0.62	0.38

compression, and not by real modelling the fibre local instability. The main differences between the two approaches are that in the first one the damage is irrecoverable and its threshold is fixed, while in the second one the local instability threshold may be recovered or alleviated if additional transversal stiffness is provided. This second approach is more appropriate but requires further development. Despite the limitations of the first approach, it is used here as an effective way of reproducing the overall behaviour.

3.5. Failure exercise

In order to perform a reliable validation procedure, the experimental data provided by the "world-wide failure exercise" [2] have been used to validate the predictions of the ESP model. All voluminous data generated by the "failure exercise" is considered to be an appropriate benchmark procedure for any model that aims to predict the mechanical response of FRP laminates. Another main contribution is the exhaustive comparison of the predictive capabilities of current failure theories for composite laminates, as reported by Soden et al. [31] and Kaddour et al. [32].

All failure envelopes are obtained by testing a hexahedral composite element, whose material properties were calibrated using the procedure defined in the previous sections. Incremental force-controlled loading scenarios are applied up to final failure.

3.5.1. Failure envelope for combined longitudinal and shear loading

Fig. 10 shows the biaxial failure envelope obtained with the ESP model, under combined longitudinal and shear loading (σ_x vs. τ_{xy}) for the E-glass/epoxy LY556 unidirectional lamina. Several stress states with different ratios σ_x:τ_{xy} were applied.

As expected, rectangular envelope is obtained. Good accordance with experiments is achieved for tensile and compressive longitudinal strengths while shear response is slightly underestimated.

3.5.2. Failure envelope for combined transverse and shear loading

The biaxial failure envelope under combined transverse and shear loading (σ_y vs. τ_{xy}) for the LY556 unidirectional lamina is illustrated in Fig. 11 as predicted by the ESP model, together with the experimental data provided by Soden et al. [29]. For comparison, the domain given by Puck and Schürmann [4] is also reported.

Good accordance with experiments is achieved for the tensile and compressive transversal strengths. The shear response is underestimated in the first quadrant probably due to inappropriate selection of the matrix failure envelope (damage surface).

3.5.3. Failure envelopes for [90°/±30°/90°] GFRP laminate

We now consider the failure envelopes for a [90°/±30°/90°] laminate made of E-glass/epoxy LY556. The precise lay-up configuration is the following: [90°/+30°/−30°/−30°/+30°/90°].

In Fig. 12, the experimental data points for failure under combined longitudinal and shear loading (σ_x vs. τ_{xy}) are reported, together with the failure envelope supplied by the ESP model prediction and Puck's estimation.

Acceptable agreement with the experimental data and Puck's envelope is achieved. We remark that in the zones where our model slightly overestimates the strength (i.e. for pure compressive σ_x and in the central zone of maximum τ_{xy}) the collapse is due to delamination and local buckling.

In Fig. 13, the experimental data points for failure under combined direct stresses (σ_x vs. σ_y) are reported, together with the failure envelope obtained by the ESP model. Failure predicted by Puck and Schürmann [4] is also reported for comparison.

The few test results carried out under external pressure and axial compression were reported to be governed by

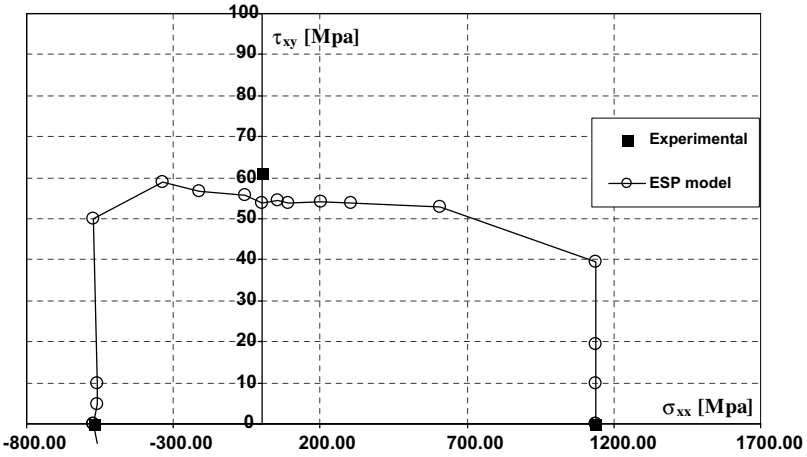

Fig. 10. Biaxial failure envelope for glass–epoxy LY556 unidirectional lamina under combined longitudinal and shear loading.

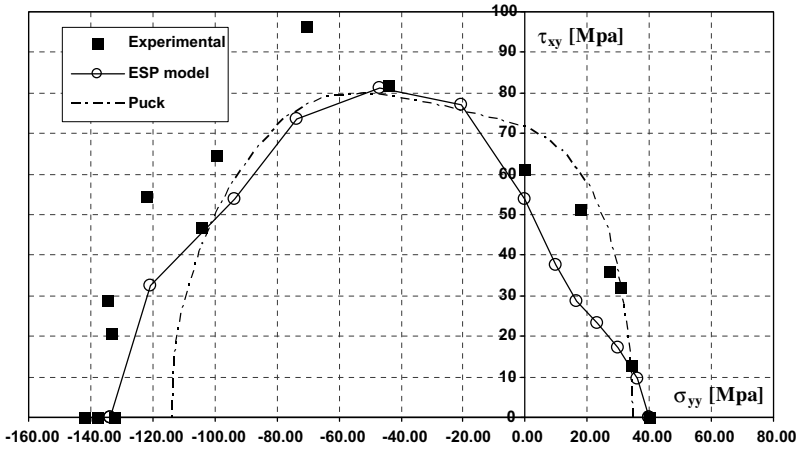

Fig. 11. Biaxial failure envelope for glass–epoxy LY556 unidirectional lamina under combined transversal and shear loading. Comparison with experimental data and the Puck's estimation.

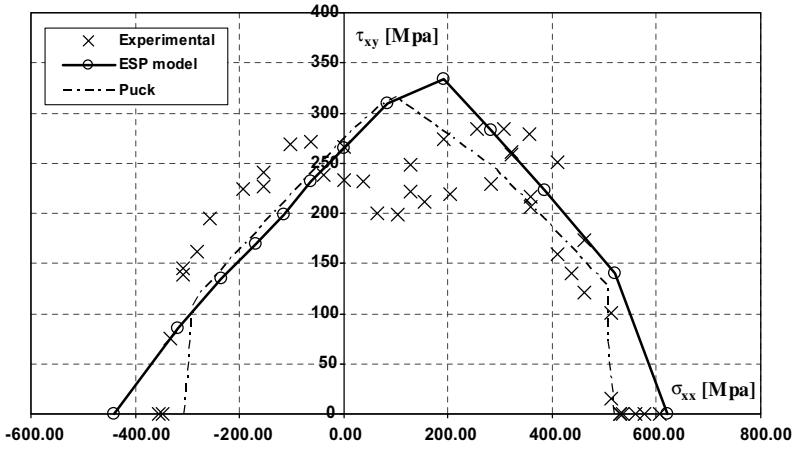

Fig. 12. Biaxial failure envelope for [90°/±30°/90°] glass–epoxy LY556 laminate under combined longitudinal and shear loading. Comparison with experimental data and the Puck's estimation.

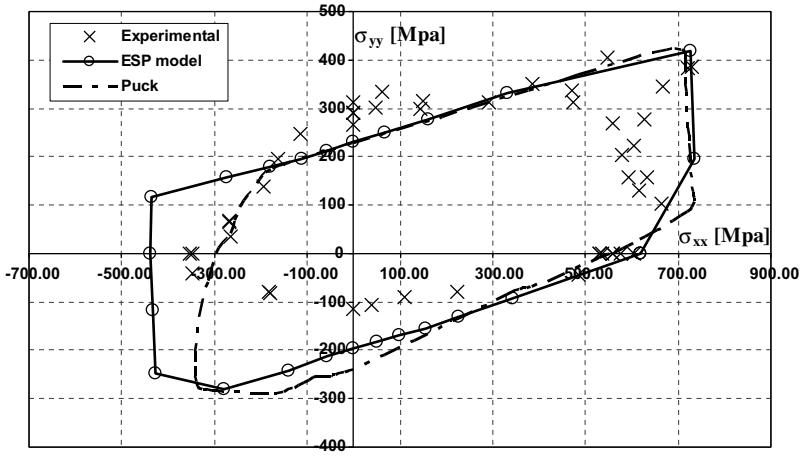

Fig. 13. Biaxial failure envelope for [90°/±30°/90°] glass–epoxy LY556 laminate under combined longitudinal and transverse loading. Comparison with experimental data and the Puck's estimation.

global buckling in the tubular specimens. Thus, in the quadrant $\sigma_x < 0$, $\sigma_y < 0$, the experimental data cannot be directly compared with the theoretical predictions, which do not take global buckling into account.

4. Concluding remarks

The serial–parallel (SP) model is combined with classical lamination theory to describe laminates consisting of unidirectional continuously reinforced layers. Its relative simplicity and the resulting numerical efficiency make the SP approach well suited for implementation as a material model in finite element programs for studying the elasto-plastic response of structures or components made of long fibre-reinforced laminated composites. In addition, it requires relatively small computational resources when implemented into a structural FE code. Its initial drawback of underestimation of the transverse and shear stiffness is then improved upon with the enriched SP model.

Quadratic convergence is achieved at local iterations whenever consistent tangent operators are provided by each component model. Quick convergence is also obtained for the global equilibrium as the algorithmic tangent operator is provided for the composite.

Validations show the capability of the ESP model to predict failure and post-failure behaviour of the composite based on appropriate constitutive models of components materials.

Comparison between experimental and numerical testing carried out on material samples enables us to state that the methodology presented here is very promising for material non-linear analysis of composite materials and structures.

Acknowledgements

This work has been partially funded by the European Commission under the GROWTH Project GRD2-2000-30091 "COMPASS", by the Spanish government through an FPU grant for F. Rastellini and through the project MAT2003-09768-C03-02 "DELCOMAR". All this support is gratefully acknowledged. We also thank R. Serpieri for his significant help with the numerical model validations during his stage at CIMNE.

Appendix. Derivation of the tangent operator

The derivation of the tangent matrix for the composite is performed by linearizing the system constituted by Eqs. (16)–(20) governing the BSP model, and by Eq. (3), which relates average stresses. Denoting the infinitesimal increments with a d prefix, the linearized system of equations reads:

$$\begin{cases} d^f\boldsymbol{\sigma} = \frac{\partial^f\boldsymbol{\sigma}}{\partial^f\boldsymbol{\varepsilon}} : d^f\boldsymbol{\varepsilon} = {}^f\mathbb{C} : d^f\boldsymbol{\varepsilon}, \\ d^m\boldsymbol{\sigma} = \frac{\partial^m\boldsymbol{\sigma}}{\partial^m\boldsymbol{\varepsilon}} : d^m\boldsymbol{\varepsilon} = {}^m\mathbb{C} : d^m\boldsymbol{\varepsilon}, \\ d\boldsymbol{\varepsilon} = {}^fk\ d^f\boldsymbol{\varepsilon} + {}^mk\ d^m\boldsymbol{\varepsilon}, \\ d^m\boldsymbol{\varepsilon}_P = d^f\boldsymbol{\varepsilon}_P, \\ d^m\boldsymbol{\sigma}_S = d^f\boldsymbol{\sigma}_S, \\ d\boldsymbol{\sigma} = {}^fk\ d^f\boldsymbol{\sigma} + {}^mk\ d^m\boldsymbol{\sigma}. \end{cases} \tag{35}$$

The above set of equations may be conveniently rearranged using decomposition (22):

$$\begin{aligned} &d^f\boldsymbol{\sigma}_P = {}^f\mathbb{C}_{PP} : d^f\boldsymbol{\varepsilon}_P + {}^f\mathbb{C}_{PS} : d^f\boldsymbol{\varepsilon}_S, \quad \text{(a)} \\ &d^f\boldsymbol{\sigma}_S = {}^f\mathbb{C}_{SP} : d^f\boldsymbol{\varepsilon}_P + {}^f\mathbb{C}_{SS} : d^f\boldsymbol{\varepsilon}_S, \quad \text{(b)} \\ &d^m\boldsymbol{\sigma}_P = {}^m\mathbb{C}_{PP} : d^m\boldsymbol{\varepsilon}_P + {}^m\mathbb{C}_{PS} : d^m\boldsymbol{\varepsilon}_S, \quad \text{(c)} \\ &d^m\boldsymbol{\sigma}_S = {}^m\mathbb{C}_{SP} : d^m\boldsymbol{\varepsilon}_P + {}^m\mathbb{C}_{SS} : d^m\boldsymbol{\varepsilon}_S, \quad \text{(d)} \\ &d\boldsymbol{\varepsilon}_P = {}^fk\ d^f\boldsymbol{\varepsilon}_P + {}^mk\ d^m\boldsymbol{\varepsilon}_P, \quad \text{(e)} \\ &d\boldsymbol{\varepsilon}_S = {}^fk\ d^f\boldsymbol{\varepsilon}_S + {}^mk\ d^m\boldsymbol{\varepsilon}_S, \quad \text{(f)} \\ &d\boldsymbol{\sigma}_P = {}^fk\ d^f\boldsymbol{\sigma}_P + {}^mk\ d^m\boldsymbol{\sigma}_P, \quad \text{(g)} \\ &d\boldsymbol{\sigma}_S = {}^fk\ d^f\boldsymbol{\sigma}_S + {}^mk\ d^m\boldsymbol{\sigma}_S, \quad \text{(h)} \\ &d^m\boldsymbol{\varepsilon}_P = d^f\boldsymbol{\varepsilon}_P, \quad \text{(i)} \\ &d^m\boldsymbol{\sigma}_S = d^f\boldsymbol{\sigma}_S. \quad \text{(j)} \end{aligned} \tag{36}$$

The solution of the previous system is obtained in a straightforward manner once $d^f\boldsymbol{\varepsilon}_S$ and $d^m\boldsymbol{\varepsilon}_S$ are separated from the remaining variables. From (36)i and e we obtain:

$$d^m\boldsymbol{\varepsilon}_P = d^f\boldsymbol{\varepsilon}_P = d\boldsymbol{\varepsilon}_P. \tag{37}$$

From (37), (36)j, b and d we deduce:

$${}^f\mathbb{C}_{SS} : d^f\boldsymbol{\varepsilon}_S = {}^m\mathbb{C}_{SS} : d^m\boldsymbol{\varepsilon}_S - ({}^f\mathbb{C}_{SP} - {}^m\mathbb{C}_{SP}) : d\boldsymbol{\varepsilon}_P. \tag{38}$$

By pre-multiplying (36)f for ${}^f\mathbb{C}_{SS}$, we get:

$${}^f\mathbb{C}_{SS} : d\boldsymbol{\varepsilon}_S = {}^fk\ {}^f\mathbb{C}_{SS} : d^f\boldsymbol{\varepsilon}_S + {}^mk\ {}^f\mathbb{C}_{SS} : d^m\boldsymbol{\varepsilon}_S. \tag{39}$$

If we substitute the expression (38) in (39), we obtain:

$$\begin{aligned} {}^f\mathbb{C}_{SS} : d\boldsymbol{\varepsilon}_S = {}^fk[{}^m\mathbb{C}_{SS} : d^m\boldsymbol{\varepsilon}_S - ({}^f\mathbb{C}_{SP} - {}^m\mathbb{C}_{SP}) : d\boldsymbol{\varepsilon}_P] \\ + {}^mk\ {}^f\mathbb{C}_{SS} : d^m\boldsymbol{\varepsilon}_S. \end{aligned}$$

By rearranging the last expression, we may highlight the term $d^m\boldsymbol{\varepsilon}_S$:

$$\begin{aligned} &({}^fk^m\mathbb{C}_{SS} + {}^mk^f\mathbb{C}_{SS}) : d^m\boldsymbol{\varepsilon}_S = {}^f\mathbb{C}_{SS} : d\boldsymbol{\varepsilon}_S + {}^fk({}^f\mathbb{C}_{SP} - {}^m\mathbb{C}_{SP}) : d\boldsymbol{\varepsilon}_P, \\ &d^m\boldsymbol{\varepsilon}_S = \mathbb{A} : [{}^f\mathbb{C}_{SS} : d\boldsymbol{\varepsilon}_S + {}^fk({}^f\mathbb{C}_{SP} - {}^m\mathbb{C}_{SP}) : d\boldsymbol{\varepsilon}_P], \end{aligned} \tag{40}$$

where $\mathbb{A} = ({}^fk\ {}^m\mathbb{C}_{SS} + {}^mk\ {}^f\mathbb{C}_{SS})^{-1}$.

By commuting indexes f and m of Eq. (40), the solution for $d^f\boldsymbol{\varepsilon}_S$ is obtained:

$$d^f\boldsymbol{\varepsilon}_S = \mathbb{A} : [{}^m\mathbb{C}_{SS} : d\boldsymbol{\varepsilon}_S + {}^mk({}^m\mathbb{C}_{SP} - {}^f\mathbb{C}_{SP}) : d\boldsymbol{\varepsilon}_P]. \tag{41}$$

The knowledge of $d^m\boldsymbol{\varepsilon}_S$ and $d^f\boldsymbol{\varepsilon}_S$ enables the composite stiffness to be obtained directly. With regard to the parallel part of composite tangent operator, the substitution of Eq. (36)a, c and (37), in Eq. (36)g yields:

$$\begin{aligned} d\boldsymbol{\sigma}_P = {}&{}^fk({}^f\mathbb{C}_{PP} : d\boldsymbol{\varepsilon}_P + {}^f\mathbb{C}_{PS} : d^f\boldsymbol{\varepsilon}_S) \\ &+ {}^mk({}^m\mathbb{C}_{PP} : d\boldsymbol{\varepsilon}_P + {}^m\mathbb{C}_{PS} : d^m\boldsymbol{\varepsilon}_S) \end{aligned}$$

and the use of (40) and (41) in the last expression finally provides:

$$\begin{aligned} d\boldsymbol{\sigma}_P = {}&{}^fk\{{}^f\mathbb{C}_{PP} : d\boldsymbol{\varepsilon}_P + {}^f\mathbb{C}_{PS} : \mathbb{A} : [{}^m\mathbb{C}_{SS} : d\boldsymbol{\varepsilon}_S \\ &+ {}^mk({}^m\mathbb{C}_{SP} - {}^f\mathbb{C}_{SP}) : d\boldsymbol{\varepsilon}_P]\} + {}^mk\{{}^m\mathbb{C}_{PP} : d\boldsymbol{\varepsilon}_P \\ &+ {}^m\mathbb{C}_{PS} : \mathbb{A} : [{}^f\mathbb{C}_{SS} : d\boldsymbol{\varepsilon}_S + {}^fk({}^f\mathbb{C}_{SP} - {}^m\mathbb{C}_{SP}) : d\boldsymbol{\varepsilon}_P]\}. \end{aligned}$$

By expanding the previous expression and rearranging the terms, one obtains:

$$\boxed{\begin{aligned} d\boldsymbol{\sigma}_P = &[({}^f k^f \mathbb{C}_{PP} + {}^m k^m \mathbb{C}_{PP}) + {}^m k^f k({}^f \mathbb{C}_{PS} - {}^m \mathbb{C}_{PS}) : \mathbb{A} : ({}^m \mathbb{C}_{SP} - {}^f \mathbb{C}_{SP})] : d\boldsymbol{\varepsilon}_P \\ &+ ({}^f k^f \mathbb{C}_{PS} : \mathbb{A} : {}^m \mathbb{C}_{SS} + {}^m k^m \mathbb{C}_{PS} : \mathbb{A} : {}^f \mathbb{C}_{SS}) : d\boldsymbol{\varepsilon}_S \end{aligned}} \tag{42}$$

As regards the serial part of composite tangent matrix, Eq. (36)h and j yield:

$$\begin{aligned} d\boldsymbol{\sigma}_S &= d^f \boldsymbol{\sigma}_S, \\ d\boldsymbol{\sigma}_S &= d^m \boldsymbol{\sigma}_S. \end{aligned} \tag{43}$$

The first equation of Eq. (43) together with (37), (36)b and (41) provides:

$$\begin{aligned} d\boldsymbol{\sigma}_S = &{}^f \mathbb{C}_{SP} d\boldsymbol{\varepsilon}_P + {}^f \mathbb{C}_{SS} : \mathbb{A} : [{}^m \mathbb{C}_{SS} : d\boldsymbol{\varepsilon}_S \\ &+ {}^m k({}^m \mathbb{C}_{SP} - {}^f \mathbb{C}_{SP}) : d\boldsymbol{\varepsilon}_P] \\ = &({}^f \mathbb{C}_{SS} : \mathbb{A} : {}^m \mathbb{C}_{SS}) : d\boldsymbol{\varepsilon}_S + [{}^f \mathbb{C}_{SP} + {}^m k^f \mathbb{C}_{SS} : \\ &\mathbb{A} : ({}^m \mathbb{C}_{SP} - {}^f \mathbb{C}_{SP})] : d\boldsymbol{\varepsilon}_P. \end{aligned} \tag{44}$$

The last expression may be set in a form invariant to commutation of indices f and m by adding the commuted expression and dividing by two. The operation yields:

$$\begin{aligned} d\boldsymbol{\sigma}_S = &\frac{1}{2}[({}^m \mathbb{C}_{SS} : \mathbb{A} : {}^f \mathbb{C}_{SS}) + ({}^f \mathbb{C}_{SS} : \mathbb{A} : {}^m \mathbb{C}_{SS})] : d\boldsymbol{\varepsilon}_S \\ &+ \frac{1}{2}({}^m \mathbb{C}_{SP} + {}^f \mathbb{C}_{SP}) : d\boldsymbol{\varepsilon}_P + \frac{1}{2}[{}^m k^f \mathbb{C}_{SS} : \mathbb{A} : ({}^m \mathbb{C}_{SP} - {}^f \mathbb{C}_{SP}) \\ &+ {}^f k^m \mathbb{C}_{SS} : \mathbb{A} : ({}^f \mathbb{C}_{SP} - {}^m \mathbb{C}_{SP})] : d\boldsymbol{\varepsilon}_P. \end{aligned} \tag{45}$$

This last expression may be strongly simplified observing that:

$$\begin{aligned} \frac{1}{2}({}^m \mathbb{C}_{SP} + {}^f \mathbb{C}_{SP}) = &\frac{1}{2}\mathbb{A}^{-1} : \mathbb{A} : ({}^m \mathbb{C}_{SP} + {}^f \mathbb{C}_{SP}) \\ = &\frac{1}{2}({}^f k^m \mathbb{C}_{SS} + {}^m k^f \mathbb{C}_{SS}) : \mathbb{A} : ({}^m \mathbb{C}_{SP} + {}^f \mathbb{C}_{SP}) \\ = &\frac{1}{2}{}^f k^m \mathbb{C}_{SS} : \mathbb{A} : {}^m \mathbb{C}_{SP} + \frac{1}{2}{}^f k^m \mathbb{C}_{SS} : \mathbb{A} : {}^f \mathbb{C}_{SP} \\ &+ \frac{1}{2}{}^m k^f \mathbb{C}_{SS} : \mathbb{A} : {}^m \mathbb{C}_{SP} + \frac{1}{2}{}^m k^f \mathbb{C}_{SS} : \mathbb{A} : {}^f \mathbb{C}_{SP}, \end{aligned} \tag{46}$$

thus, Eq. (45) arrives at its final expression:

$$\boxed{\begin{aligned} d\boldsymbol{\sigma}_S = &\tfrac{1}{2}[({}^m \mathbb{C}_{SS} : \mathbb{A} : {}^f \mathbb{C}_{SS}) + ({}^f \mathbb{C}_{SS} : \mathbb{A} : {}^m \mathbb{C}_{SS})] : d\boldsymbol{\varepsilon}_S \\ &+ ({}^m k^f \mathbb{C}_{SS} : \mathbb{A} : {}^m \mathbb{C}_{SP} + {}^f k^m \mathbb{C}_{SS} : \mathbb{A} : {}^f \mathbb{C}_{SP}) : d\boldsymbol{\varepsilon}_P \end{aligned}} \tag{47}$$

The remarked expressions (42) and (47) are used to obtain the composite tangent operator Eq. (29), which results in terms of the components constitutive tangent tensors.

References

[1] Rastellini F. Modelización numérica de la no-linealidad constitutiva de laminados compuestos. PhD thesis. ETSECCPB. Politechnical University of Catalonia, Barcelona, March, 2006 [in Spanish].

[2] Hinton MJ, Soden PD. Predicting failure in composite laminates: the background to the exercise. Comp Sci Technol 1998;58:1001–10.

[3] Liu KS, Tsai SW. A progressive quadratic failure criterion for a laminate. Comp Sci Technol 1998;58:1023–32.

[4] Puck A, Schürmann H. Failure analysis of FRP laminates by means of physically based phenomenological models. Comp Sci Technol 1998;58(7):1045–67.

[5] Puck A, Schürmann H. Failure analysis of FRP laminates by means of physically based phenomenological models. Comp Sci Technol 2002;62:1633–62.

[6] Oller S, Miquel J, Zalamea F. Composite material behavior using a homogenization double scale method. J Eng Mech 2005;131(1):65–79.

[7] Car E, Zalamea F, Oller S, Miquel J, Oñate E. Numerical simulation of fiber reinforced composite materials. Int J Solids Struct 2002;39:1967–86.

[8] Voigt W. Über die Beziehung zwischen den beiden Elasticitäts-Constanten isotroper Körper. Ann Phys 1889;38:573–87 [in German].

[9] Reuss A. Berechnung der Fliebgrenze von Mischkristallen auf grund der Plastizitätsbedingung für Einkristalle. ZAMM 1929;9:49–58 [in German].

[10] Trusdell C, Toupin R. The classical field theories. Berlin: Springer Verlag; 1960.

[11] Green AE, Naghdi PM. A dynamical theory of interacting continua. Int J Eng Sci 1965;3:231–41.

[12] Ortiz M, Popov EP. Plain concrete as a composite material. Mech Mater 1982;1(2):139–50.

[13] Ortiz M, Popov EP. Physical model for the inelasticity of concrete. Proc Roy Soc London 1982;A383:101–25.

[14] Oller S, Oñate E, Miquel J, Botello S. A plastic damage constitutive model for composite materials. Int J Solids Struct 1996;33(17):2501–18.

[15] Neamtu L, Oller S, Oñate E. A generalized mixing theory elasto-damage-plastic model for finite element analysis of composites. In: Owen DR, Oñate E, Hinton E, editors. COMPLAS V – 5th International Conference on Computational Plasticity. Barcelona: CIMNE; 1997.

[16] Car E, Oller S, Oñate E. Anisotropic elastoplastic constitutive model for large strain analysis of fiber reinforced composite materials. Comput Methods Appl Mech Eng 2000;185:245–77.

[17] Rastellini F, Oller S, Salomon O, Oñate E. Advanced serial–parallel mixing theory for composite materials analysis. Continuum basis and finite element applications. In: Proceeding of the VII international conference on computational plasticity, COMPLAS 2003. Barcelona: CIMNE [on CD].

[18] Rastellini F, Oller S, Salomon O, Oñate E. Teoría de mezclas Serie-Paralelo avanzada para el análisis de materiales compuestos. In: Miravete A, Cuartero J, editors. Proceedings of AEMAC 2003. Zaragoza (Spain), p. 729–41 [in Spanish].

[19] Rastellini F, Oller S. Modelado numérico de no linealidad constitutiva en laminados compuestos – Teoría de mezclas. In: Métodos Computacionais em Engenharia. APMTAC 2004, Lisbon (Portugal) [on CD, in Spanish].

[20] Salomón O, Rastellini F, Oller S, and Oñate E. Fatigue prediction for composite materials and structures. NATO Symposium AVT–121, Granada (Spain), October 2005.

[21] Dvorak GJ, Bahei-El-Din YA. Plasticity analysis of fibrous composites. ASME Trans J Appl Mech 1982;49:327–35.

[22] Hill R. Theory of mechanical properties of fibre-strengthened materials: I. elastic behaviour. J Mech Phys Solids 1964;12:199–212.

[23] Reddy JN. Mechanics of laminated composite plates and shells – theory and analysis. 2nd ed. New York: CRC Press; 2004.

[24] Barbero EJ. Introduction to composite materials design. London: Taylor & Francis; 1998.

[25] Halpin JC, Tsai SW. Effects of environmental factors on composite materials. Air Force Materials Lab-Technical report 67-423, Department of Defense (USA), 1969.

[26] Jones RM. Mechanics of composite materials. London: Taylor & Francis; 1999.

[27] Faria R, Oliver J, Cervera M. A strain-based plastic viscous-damage model for massive concrete structures. Int J Solids Struct 1998;35(14):1533–58.
[28] Soden PD, Hinton MJ, Kaddour AS. Lamina properties, lay-up configurations and loading conditions for a range of fibre-reinforced composite laminates. Comp Sci Technol 1998;58:1011–22.
[29] Soden PD, Hinton MJ, Kaddour AS. Biaxial test results for strength and deformation of a range of E-glass and carbon fibre reinforced composite laminates: failure exercise benchmark data. Comp Sci Technol 2002;62:1489–514.
[30] Hütter U, Schelling H, Krauss H. An experimental study to determine failure envelope of composite materials with tubular specimen under combined loads and comparison between several classical criteria. In: Failure modes of composite materials with organic matrices and other consequences on design. NATO, AGRAD, conference proceedings No. 163, Munich (Germany), pp. 13–19. 1974.
[31] Soden PD, Hinton MJ, Kaddour AS. A comparison of the predictive capabilities of current failure theories for composite laminates. Comp Sci Technol 1998;58:1225–54.
[32] Kaddour AS, Hinton MJ, Soden PD. A comparison of the predictive capabilities of current failure theories for composite laminates: additional contributions. Comp Sci Technol 2004;64:449–76.